HHS Public Access

Author manuscript

Cell Rep. Author manuscript; available in PMC 2022 October 05.

Published in final edited form as:

Cell Rep. 2022 September 20; 40(12): 111389. doi:10.1016/j.celrep.2022.111389.

Targeting the succinate receptor effectively inhibits periodontitis

Yuqi Guo[1,8], **Fangxi Xu**[1,8], **Scott C. Thomas**[1], **Yanli Zhang**[1], **Bidisha Paul**[1], **Satish Sakilam**[2], **Sungpil Chae**[1], **Patty Li**[1], **Caleb Almeter**[1], **Angela R. Kamer**[3], **Paramjit Arora**[2], **Dana T. Graves**[4], **Deepak Saxena**[1,5,*], **Xin Li**[1,6,7,9,*]

[1]Department of Molecular Pathobiology, New York University College of Dentistry, New York, NY 10010, USA

[2]Department of Chemistry, New York University, New York, NY 10003, USA

[3]Department of Periodontology and Implant Dentistry, New York University College of Dentistry, New York, NY 10010, USA

[4]Department of Periodontics, University of Pennsylvania School of Dental Medicine, Philadelphia, PA 19104, USA

[5]Department of Surgery, New York University Grossman School of Medicine, New York, NY 10016, USA

[6]Department of Urology, New York University Grossman School of Medicine, New York, NY 10016, USA

[7]Perlmutter Cancer Institute, New York University Langone Medical Center, New York, NY 10016, USA

[8]These authors contributed equally

[9]Lead contact

SUMMARY

Periodontal disease (PD) is one of the most common inflammatory diseases in humans and is initiated by an oral microbial dysbiosis that stimulates inflammation and bone loss. Here, we report an abnormal elevation of succinate in the subgingival plaque of subjects with severe PD. Succinate activates succinate receptor-1 (SUCNR1) and stimulates inflammation. We detected SUCNR1 expression in the human and mouse periodontium and hypothesize that succinate activates SUCNR1 to accelerate periodontitis through the inflammatory response. Administration

*Correspondence: ds100@nyu.edu (D.S.), xl15@nyu.edu (X.L.).

AUTHOR CONTRIBUTIONS

Conceptualization, Y.G., F.X., D.S., and X.L.; methodology, Y.G., D.S., and X.L.; investigation, Y.G., F.X., S.C.T., Y.Z., B.P., S.C., C.A., and P.L.; formal analysis, Y.G., F.X., S.T., and S.S.; writing – original draft, Y.G., F.X., S.S., D. S., and X.L.; writing – review & editing, S.T., D.T.G., D.S., and X.L.; funding acquisition, D.T.G., D.S., and X.L.; resources, S.S., P.A., and A.R.K.; supervision, D.S. and X.L. All authors approved the manuscript.

SUPPLEMENTAL INFORMATION

Supplemental information can be found online at https://doi.org/10.1016/j.celrep.2022.111389.

DECLARATION OF INTERESTS

D. S. and X.L. are co-founders of Periomics Care LLC.

of exogenous succinate enhanced periodontal disease, whereas SUCNR1 knockout mice were protected from inflammation, oral dysbiosis, and subsequent periodontal bone loss in two different models of periodontitis. Therapeutic studies demonstrated that a SUCNR1 antagonist inhibited inflammatory events and osteoclastogenesis *in vitro* and reduced periodontal bone loss *in vivo*. Our study reveals succinate's effect on periodontitis pathogenesis and provides a topical treatment for this disease.

Graphical Abstract

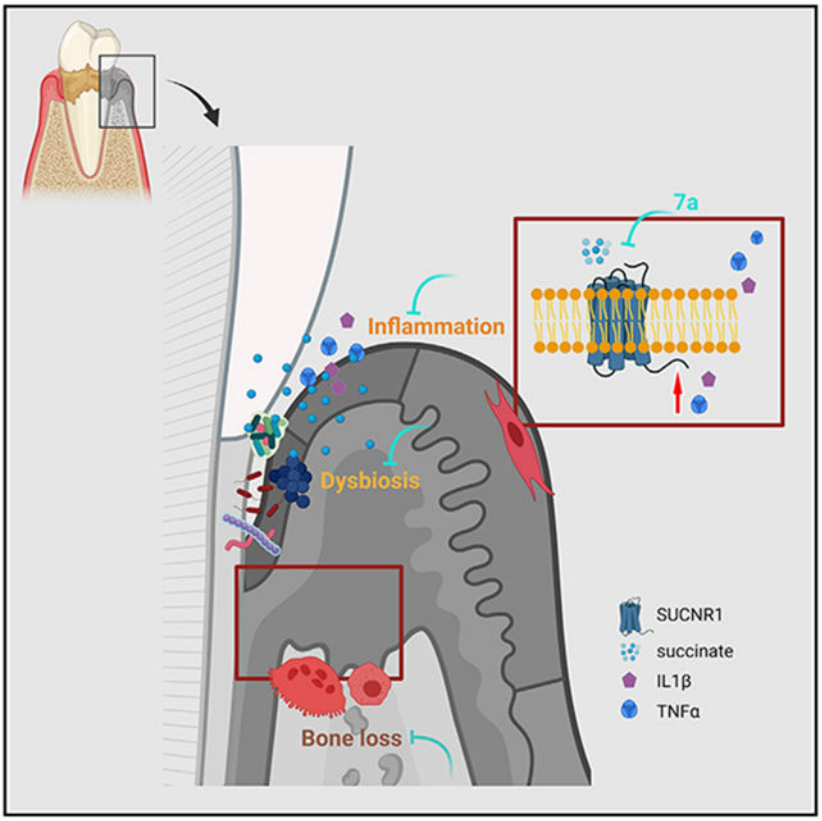

In brief

Periodontitis is the most prevalent adult oral disease. Guo et al. show elevation of succinate in periodontitis, which aggravates the disease through the succinate receptor (SUCNR1). They developed a gel formulation of a small compound specifically blocking SUCNR1 to prevent and treat periodontitis by inhibiting dysbiosis, inflammation, and bone loss.

INTRODUCTION

Periodontal disease (PD) is a common chronic inflammatory disease that is highly prevalent and negatively affects the quality of life. PD affects up to half of adults and is induced by a bacterial dysbiosis in the oral cavity that stimulates inflammation (Eke et al., 2015; Nazir, 2017). In more severe forms, PD leads to loss of bone that is functionally needed to support teeth during mastication. The role of the microbial biofilm in PD is well established

(Socransky et al., 1998). Under healthy conditions, the oral microbiome harbors hundreds of bacterial species that exhibit a homeostatic equilibrium with the host (Zaura et al., 2009). When this ecological balance is disturbed, interactions between the microbiota and host response are disturbed and may lead to tissue destruction and systemic dissemination of bacteria (Correa et al., 2019; Ganther et al., 2021; Hajishengallis, 2015; Hoare et al., 2019; Kilian et al., 2016; Lamont et al., 2018; Olsen and Yamazaki, 2019; Suarez et al., 2020). Several metabolic products may affect host-bacteria interactions to promote pathogenesis. One of these could be succinate, a key intermediate metabolite in the Krebs cycle. An association between increased succinate levels in gingival crevicular fluid and periodontitis has been reported more than three decades ago (Ohwaki, 1988), but a causal relationship between succinate and PD has not been established, and a route for a potential therapeutic benefit has not been explored.

We have recently reported a link between elevated succinate levels and diabetes (Li et al., 2015) and stimulation of osteoclast formation by succinate (Guo et al., 2017). These findings may be highly significant to the pathogenesis of PD, considering that diabetic individuals have increased susceptibility to periodontitis (Graves et al., 2007, 2020). Accumulation of succinate in the mitochondria, cytosol, and extracellular environment has been observed in several pathophysiological states (Li et al., 2015; Littlewood-Evans et al., 2016; Rubic-Schneider et al., 2017; Sadagopan et al., 2007; Serena et al., 2018; Tannahill et al., 2013; Toma et al., 2008). Succinate accumulation occurs when there is an imbalance between energy demand and oxygen supply (Chouchani et al., 2014; Lewis et al., 2010). Accumulation could be a direct consequence of reduced succinate dehydrogenase activity in the host cells (Guo et al., 2017; Krebs, 1970; Li et al., 2015). Succinate first accumulates in mitochondria and then the cytosol and is eventually released to the extracellular environment, where it activates SUCNR1 on the target cells through autonomous or non-autonomous modes. Succinate activation of SUCNR1 is associated with multiple diseases, including diabetic retinopathy (Toma et al., 2008), hypertension (He et al., 2004; Sadagopan et al., 2007), cardiomyocyte hypertrophy (Aguiar et al., 2014), ulcerative colitis, and rheumatoid arthritis, through enhanced inflammation mediated by an increased innate inflammatory response (Fukui et al., 1997; Littlewood-Evans et al., 2016; Mills et al., 2016; Rubic-Schneider et al., 2017; Tannahill et al., 2013). Bacterial production of succinate can increase virulence gene expression (Grenier, 1992; Grenier and Mayrand, 1986; Lu et al., 2015; Tan et al., 2014), suggesting that an excess of this metabolite may initiate a shift toward a pathogenic lifestyle in the microbiota. Succinate and butyrate levels in periodontal pockets significantly correlate with clinical measures of inflammation and disease severity (Lu et al., 2014; Niederman et al., 1997; Qiqiang et al., 2012).

We uncover a mechanistic connection between increased succinate levels and periodontitis. Through gain- and loss-of-function approaches, we show that succinate modulates the host response and oral microbial community structure to affect pathogenicity. These changes paralleled those that occurred in human PD. The mechanistic studies led to development of a specific succinate receptor antagonist that reduced inflammation and prevented periodontal bone loss, demonstrating clear therapeutic value.

RESULTS

Succinate elevation contributes to periodontitis progression

Individuals with severe periodontitis have elevated succinate levels and dysbiosis of the oral microbiota in their dental plaque. Targeted metabolomic analysis of 28 gingival plaque samples collected from individuals (21 male and 7 female) without periodontitis (normal or mild gingivitis, N = 12) or severe periodontitis (N = 16) showed that the severe periodontitis group exhibited significantly elevated succinate levels (Figure 1A). The association of systemic elevation of succinate with periodontitis was recapitulated in mice (Figure 1B) with induced experimental periodontitis. This experimental periodontitis model was initiated by a 5-day placement of a ligature around the second maxillary molar tooth, followed by oral inoculation of *Fusobacterium nucleatum* to promote prolonged inflammation and dysbiosis. *F. nucleatum* can act as an anchoring perio-pathogen to initiate and support periodontitis biofilm formation (Foster and Kolenbrander, 2004; Park et al., 2016; Thurnheer et al., 2019; Yamada et al., 2005; Yip et al., 2021) and induce chronic inflammation and immune evasion locally and systemically (Hajishengallis and Chavakis, 2021; McIlvanna et al., 2021). Thus, by adapting the traditional ligature-induced PD model, we can examine initiating events in PD and later events because of prolonged inflammation and dysbiosis. Development of periodontitis involves three major components: (1) pathogen colonization, (2) chronic inflammation, and (3) bone loss. It is intriguing to investigate the expression of SUCNR1 in periodontal tissue and whether succinate elevation regulates all or some of these 3 components via activation of its receptor, SUCNR1. We initially detected expression of SUCNR1 in the periodontium of human (Figure 1C) and mouse (Figures 1D and 1E) by immunohistochemistry and immunofluorescence staining, respectively. We also confirmed expression of SUCNR1 in human gingival fibroblasts by immunofluorescence staining (Figure S1A). *SUCNR1* gene expression was detected in murine oral mucosal epithelial tissue by *in situ* hybridization using RNAScope (Figure 1F) and real-time PCR (PCR) (Figure S1B). The *SUCNR1* mRNA levels remained similar between the healthy periodontium tissues and periodontitis-affected tissues of mice (Figure S1C).

Next, to determine whether SUCNR1 is functionally important in PD, age-matched wild type (WT) and SUCNR1 knockout (KO) mice were randomly divided into sham or PD groups, as illustrated in Figure 2A. WT mice induced with PD (WT_Perio) exhibited more significant bone loss and more osteoclasts in the affected alveolar bone area than WT mice that received the sham treatment (WT_Healthy) (Figures 2B-2E). The bone loss and osteoclast numbers of the SUCNR1 KO mice that received PD induction (KO_Perio) were significantly less than that of WT_Perio group (Figures 2B-2E). Protection from bone loss in KO mice was detected immediately after 5-day ligature (Figures S2A and S2B). Induction of systemic inflammation, indicated by serum inflammatory cytokines, including tumor necrosis factor alpha (TNF-α) (Figure 2F), interleukin-1β (IL-1β) (Figure 2G), keratinocyte chemoattractant (KC)/human growth-regulated oncogene (GRO), IL-2, IL-6, and IL-12p70 (Figures S2C-S2F) was observed in WT_Perio mice but not in KO_Perio mice. The inflammation in the local gingival tissue increased by PD in WT and KO mice, whereas the KO_Perio group showed a trend of reduced induction of *TNF-α* mRNA (p =

0.1; Figure 2H) and a significantly reduced induction of *IL-1β* mRNA than the WT_Perio group (Figure 2I).

We examined the alpha diversity of the microbiota using oral swab samples collected from these animals. WT mice with ligature/bacterial inoculation-induced periodontitis had significantly higher amplicon sequence variant richness and evenness than the WT control group, whereas the alpha diversity in KO mice was similar in the control and ligature/bacterial inoculation groups (Figure 2J). Principal coordinates analysis (PCoA) for beta diversity showed that the WT and KO mouse microbial communities were significantly different, and WT and KO mice clearly clustered separately, based on the Bray-Curtis dissimilarity matrix (Figure 2K). The pairwise comparisons within the same genotype showed that periodontitis induced significantly different beta diversity in WT mice only (Figure S2G). The beta diversity was significantly different in WT_Perio and KO_Perio mice (Figure S2H).

At the phylum level, the relative abundance of Bacteroidetes and Saccharibacteria (TM7) was significantly higher in WT_Perio mice compared with the WT control group (Figures S2I and S2J). In contrast, the relative abundance of phyla between KO mice and KO_Perio mice remained similar. At the genus level, the heatmap of the 20 most relatively abundant genera revealed clearly different taxon abundance patterns in WT and KO mice (Figure 2L). A major shift in community structure was observed from WT control mice to WT_Perio mice but not from KO control mice to KO_Perio mice (Figure 2L). The heatmap of the top 40 relatively abundant genera in WT mice indicated an enrichment of periodontal pathogens such as *Fusobacterium* (Figure S2K). Samples of KO mice exhibited less variability and indicated an overall lower relative abundance of periodontal pathogens (Figure 2L). This PD model led to a bacterial shift toward pathogenicity in WT mice, whereas no major bacterial shift was induced in SUCNR1 KO mice.

Succinate application accelerates periodontitis

As a gain-of-function approach, we applied succinate to WT and KO mice when PD was induced through ligature and *F. nucleatum* inoculation to establish a cause-and-effect relationship between succinate elevation and the pathogenesis of periodontitis (Figure 3A). Systemic administration of succinate increased periodontal bone loss in the WT group (Figures 3B and 3C). In contrast, SUCNR1 KO mice were resistant to succinate treatment and exhibited bone loss similar to the control group treated with Dulbecco's phosphate-buffered saline (PBS), with PBS-treated KO mice even displaying reduced bone loss with respect to the PBS-treated WT mice. A similar relationship was observed in a lipopolysaccharides (LPS)-induced periodontal bone loss model (Figure S3A), where local application of LPS induced periodontal bone loss in WT mice and was enhanced by systemic succinate injection. Thus, application of succinate significantly enhanced LPS-induced periodontal bone loss in WT mice but had little effect in SUCNR1 KO mice (Figure S3B).

We next investigated the effect of systemic application of succinate on the oral microbiota by 16S sequencing. The boxplots for alpha diversity measurements (Figure 3D) and PCoA analysis for beta diversity (Figure 3E) remained similar for succinate and PBS treatment

in WT and KO mice. It indicates that application of succinate does not drive significant changes in the oral bacterial community. We examined the taxonomic profiles (Figure 3F) and phylum-level relative abundance (Figure S4A), which supported a significant increase in Saccharibacteria (TM7) in WT mice that received succinate injections. To assess whether succinate can directly support growth of periodontal pathogens, we cultured *F. nucleatum* in medium supplemented with various concentrations of succinate. The growth rate and maximum cell density of *F. nucleatum* significantly increased with increasing succinate concentrations, and maximum growth was observed for 100 μM 24.5 h after inoculation (0.504 ± 0.016, optical density 600 [OD_{600}], $6.25 \pm 0.2 \times 10^6$ colony-forming units [CFUs/mL]) (Figure 3G). Succinate significantly increased the expression of virulence factors coding for hemolysin, a Lys R family transcriptional regulator; hemolysin-related protein; and Hemin receptor of *F. nucleatum* (Figures S4B-S4E).

Development and validation of a SUCNR1 antagonist *in vitro*

Our results strongly indicate that activation of SUCNR1 by elevated succinate facilitates manifestation of periodontitis, whereas the absence of SUCNR1 and, thus, its activity significantly reduces susceptibility to periodontitis. To test the therapeutic potential of this observation, we developed a specific antagonist of SUCNR1. As shown in Figure 4A, we synthesized a specific antagonist of SUCNR1 (7a) and established its purity by high-performance liquid chromatography (HPLC), as shown in Figure 4B. To confirm that the antagonist can suppress activation of SUCNR1, we used a calcium flux FLIPR assay for cells expressing the human SUCNR1 in Chem-1 host cells. We observed that 7a efficiently suppressed succinate-induced SUCNR1 activation. The inhibitory effects of 7a started as low as 5 μM and increased in a dose-dependent manner (Figure 4C). To assess whether 7a blocked biological activity induced by succinate, we examined its capacity to inhibit succinate-induced osteoclastogenesis *in vitro*. 7a caused dose-dependent abolishment of succinate-stimulated osteoclastogenesis (Figures 4D and 4E). Similarly, the 7a antagonist reduced LPS-induced TNF-α and IL-1β expression (Figures 4F and 4G) in HGF1 cells, whereas incubation with 7a alone produced no effect.

Inhibition of periodontitis by a SUCNR1 antagonist *in vivo*

To evaluate the efficacy of 7a *in vivo*, we used a vehicle of the polymer polylactic-co-glycolic acid (PLGA) and glimepiride (GMD), referred to as *in situ* gel (ISG) formulations. The 7a/polymer combination was tested *in vivo* using a ligature combined with *F. nucleatum* inoculation model of PD that was enhanced by succinate administration (Figure 5A). The 7a/polymer formulation was applied topically every other day for 28 days, which caused a marked reduction in average alveolar bone loss. In vehicle-treated mice, the average bone loss was greater than 2-fold of that in 7a-treated mice (Figures 5B and 5C). We also assessed the effect of 7a administration on proinflammatory gene expression in the ligature-induced periodontitis model with a short-term treatment regimen consisting of three topical applications of 7a in a week (Figure 5D). A more than 30% reduction of alveolar bone loss was observed in mice treated with 7a compared with vehicle-treated mice (Figures 5E and 5F). Topical 7a application also resulted in a significant reduction in TNF-α and IL-1β expression locally in the gingival tissues (Figures 5G and 5H) and systemically in the serum (Figures 5I and 5J).

We also investigated the effect of the SUCNR1 antagonist on the oral microbiota (Figure 6). Without affecting alpha diversity (Figure 6A), treatment with 7a significantly altered the samples' PCoA for beta diversity, measured by Bray-Curtis dissimilarity of the oral microbial community (Figure 6B). Phylum-level stacked boxplots (Figure 6C) showed the community composition for the vehicle- and 7a-treated groups, with the relative abundance of Bacteroidetes depleted in the 7a-treated group. A heatmap of the 20 most relatively abundant genera (Figure 6D) also showed that 7a treatment changed the microbial community composition. The abundance of the genera *Bacteroides* and *Clostridium* was significantly greater in the vehicle group compared with the 7a-treated group. However, there was no significant change in non-PD-related bacteria in the 7a-treated group (Figure S5A). In addition to *Bacteroides* and *Clostridium*, *Sutterella*, *Ruminococcus* and *Proteus*, *Clostridium*, *Adlercreutzia*, and *Allobaculum* also tended to be less abundant in the 7a group (Figure S5A). PCR analysis confirmed *Bacteroides* reduction by 7a (Figure S5B). Linear discriminate analysis (Figures 6E and 6F) revealed a change in microbial composition induced by 7a, as reflected by 24 significantly discriminative taxa with a linear discriminant analysis (LDA) score greater than 2. Cyto-scape-generated network analysis indicates clear partitioning of features between samples from the vehicle- and the 7a- treated groups (Figure 6G). These data indicate that blocking SUCNR1 activation with 7a significantly changes the oral microbial community composition by causing a significant decrease in pathobionts.

It is important to determine whether such a relationship between succinate levels and the oral microbiota can be established in individuals with periodontitis. We examined the bacterial community in human dental plaque by comparing their alpha and beta diversity. Subjects with severe periodontitis had a significantly different bacterial composition, as determined by both parameters (Figures S6A and S6B). The relative abundance of taxonomic clades harboring periodontal pathogens (such as the phyla Bacteroidetes, Fusobacteria, and Saccharibacteria (TM7); the family Spirochaetaceae, and the genus *Treponema*) increased in individuals with severe periodontitis (Figures S6C-S6E). To study the correlations in microbiota and succinate levels, we identified the 40 most relatively abundant genera (Figure 7A) and applied Spearman's rank correlation coefficient for comparing the relative abundance of genera and succinate levels (Figures 7B and S6F). Positive correlations between succinate levels and many PD-associated bacteria, such as Bacteroidetes, *Porphyromonas*, Saccharibacteria, *Treponema*, and *Fusobacterium* (Figures 6C and S6F), were observed. A significantly stronger correlation was observed between succinate and *Prevotella*, a succinate-producing bacterium (De Vadder et al., 2016); *Lachnoanaerobaculum* (Clostridia) (Hedberg et al., 2012); *Anaeroglobus*, a novel member of the family Veillonellaceae (Ferreyra et al., 2014; Janssen, 1992); and *Atopobium* (Ceccarani et al., 2019), known to be associated with high concentrations of succinate and dysbiosis. An inverse relation between succinate level and the non-periodontal pathogens *Rothia*, *Streptococcus*, *Neisseria*, *Haemophilus*, *Actinomyces*, and *Lautropia* was observed.

Gain of function by succinate application and loss of function by SUCNR1 deletion or SUCNR1 blockage with 7a indicate that succinate plays a significant role in enhancing susceptibility to periodontitis. Mechanistically, succinate contributed to a dysbiosis of the oral microbiota, enhanced inflammatory cytokine expression (notably TNF-α and IL-1β), and promoted alveolar bone loss in ligature- and LPS-induced periodontal bone loss models.

The therapeutic implications of these findings were demonstrated by treatment with a SUCNR1 antagonist, 7a. Topical application of a 7a gel formulation effectively inhibited inflammation, dysbiosis, and bone loss in mice with periodontitis (Figure 7C).

DISCUSSION

The studies presented in this report show that succinate is a major driver of periodontitis. Inhibition of its action by targeting its receptor by genetic deletion or a therapeutic antagonist inhibits the clinical effect of PD, as measured by inflammatory cytokine expression and periodontal bone loss. We undertook a detailed microbiological analysis of the effect of succinate elevation by several approaches, including correlation analysis with succinate levels in human subjects, gain of function by application of exogenous succinate, and loss of function by SUCNR1 KO and treatment with a SUCNR1 antagonist. This analysis is important because bacteria are the critical triggers of PD, and the systemic consequences of PD are derived from dissemination of the oral bacteria systemically. Bacteria belonging to the phylum Bacteroidetes was depleted with 7a treatment. In addition, enrichment in clades harboring periodontal pathogens, including Porphyromonadaceae, *Treponema*, *Prevotella*, and Saccharibacteria taxa, was observed in vehicle-treated group. These bacteria are linked to periodontal breakdown involving bone destruction (Castro et al., 2017; Curtis et al., 2020; Ebersole et al., 1995; Marttila et al., 2014; Rosen et al., 1995). The results of these analyses establish that succinate and SUCNR1 play an essential and critical role in modifying the oral microbial community composition in a way that is consistent with increased periodontitis in mice and humans.

Succinate can be produced by host cells in response to inflammatory stimuli (Guo et al., 2020; Mills and O'Neill, 2014) as well as through fermentation by the members of the microbial community (Ferreyra et al., 2014; McDonald and White, 2019). The elevation of succinate observed in individuals with severe periodontitis is likely due to a combined increase in succinate production by host cells and bacteria. *Treponema denticola*, an oral spirochete, produces succinate as a metabolic byproduct, which can then be metabolized further by other community members, such as the oral pathogen *Porphyromonas gingivalis* in the Bacteroidetes (Grenier, 1992; Tan et al., 2014). Other oral pathogens, such as *Prevotella*, which is highly correlated with succinate levels in affected individuals, is known to produce succinate (Takahashi and Yamada, 2000).

It is plausible that an amplification cycle induces the following steps: (1) periodontal pathogens and host cells produce succinate, (2) the bacterial composition is altered to induce dysbiosis, (3) succinate and bacterial dysbiosis promote expression of inflammatory cytokines and induce bone loss, and (4) inflammation further contributes to dysbiosis. When produced and released, succinate can affect bacteria and host cells in a direct manner. We showed that succinate can stimulate the growth rate and cell yield of the oral pathogen *F. nucleatum* in a dose-dependent manner, supporting a direct effect of succinate on a periodontal pathogen. It is possible that the changes in bacterial composition may be secondary to changes in inflammation. A key finding is that, by use of the LPS-injection model, we can show that the kKO of the succinate receptor can reduce bone loss by directly reducing inflammation.

In host cells such as gingival epithelium and myeloid lineage cells that express SUCNR1, elevation of succinate stimulates release of pro-inflammatory cytokines that eventually lead to tissue damage and bone resorption. Our data showed that SUCNR1 mRNA levels remained stable in mice with periodontitis. It suggests that activation of the receptor by elevated levels of succinate, rather than the density of SUCNR1, contributed to manifestation of the disease in mice. However, whether SUCNR1 expression is altered by inflammation in individuals with periodontitis needs further investigation. SUCNR1 mRNA expression has been reported to increase in human myometrial cells by TNF-α and IL-1β (Lim and Lappas, 2020), and SUCNR1 mRNA expression in cancer cell lines can be induced by glutamine because of high respiratory rates (Rabe et al., 2022). Succinate can also mediate or enhance the interaction between pathogens and host responses. It has been shown recently that *P. gingivalis* can induce metabolic changes in periodontal ligament cells, resulting in succinate accumulation and expression of pro-inflammatory cytokines (Su et al., 2020).

We modified the conventional PD ligature model to emphasize initiation of periodontitis (ligature alone, 5 days) and the effect of prolonged bacterially induced inflammation. This approach solves a significant limitation of the short-term ligature model, which represents events that initiate periodontal bone loss but does not reflect the effect of chronic inflammation. Thus, by adapting the traditional model, we are able to examine initiating events in PD and later events because of prolonged inflammation and dysbiosis. It is significant that SUCNR1 KO mice are protected from LPS-induced bone loss. This result underscores the importance of succinate in modifying the host response in promoting the pathogenesis of periodontitis. In the LPS-induced periodontal bone loss model, bone resorption occurs within days of LPS injection and is independent of the oral microbiota (Kassem et al., 2015). Modulating host responses by enhancing or suppressing inflammation has been shown to directly affect the pathogenicity of the microbiota (Xiao et al., 2017). The changes in the microbiome of SUCNR1 KO and 7a-treated mice support the effect of inflammation, induced by succinate activation of SUCNR1, on the pathogenicity of microbiota. It is plausible that 7a is able to impede periodontal bone loss independent of its effect on the microbiome. Future studies in germ-free animals will be needed to definitively determine whether 7a functions independent of the microbiome.

We found that individuals with severe PD had an abnormal elevation of succinate in their dental plaque and that the level of succinate was proportional to the extent of PD. We undertook mechanistic studies in mouse models to determine whether succinate could lead to more severe PD. Addition of exogenous succinate altered the oral bacterial pathogenesis, causing a shift toward an increase in periodontal pathogens, enhanced periodontal inflammation, and bone resorption. Treatment with a SUCNR1 antagonist reduced formation of a dysbiotic microbiome, periodontal inflammation, and bone loss induced by oral inoculation of periodontal pathogens. Currently no treatment is available that simultaneously reduces inflammation, prevents bacterial dysbiosis, and periodontal bone loss.

Limitations of the study

Despite the reduced periodontitis symptoms having been observed in male and female SUCNR1 KO mice, not all of the experiments in the current study were performed with both sexes of mice. We adapted the ligature model by addition of a more chronic bacterial infection component to closely mimic the *in vivo* situation and allow a longer period of disease-relevant outcomes to be measured. Further adaptation of this model by addition of other periodontal pathogens, such as *P. gingivalis*, in both sexes of mice simultaneously can help to validate the findings. The current study demonstrates SUCNR1 expression in the human periodontium, but whether expression of SUCNR1 is upregulated in individuals with periodontitis and directly contributes to disease manifestation is not clear. Future clinical studies with tissue samples from large cohorts of individuals with and without periodontitis are warranted.

STAR★METHODS

RESOURCE AVAILABILITY

Lead contact—Further information and requests for resources and reagents should be directed to the lead contact and corresponding author, Xin Li (xl15@nyu.edu).

Materials availability

- The method of Compound 7a synthesis is provided in this study.
- The animal line generated in this study can be shared with the research community with proper Material Transfer Agreement through New York University.

Data and code availability

- Raw sequence data have been made publicly available on NCBI database. The accession number is listed in the Key resources table.
- All original code has been deposited at Zenodo and is publicly available as of the date of publication. The DOI is listed in the Key resources table.
- Any additional information required to reanalyze the data reported in this paper is available upon request from the corresponding author, XL.

EXPERIMENTAL MODEL AND SUBJECT DETAILS

Study design—The objective of this study was to identify the pathogenic role of succinate signaling, and therapeutic potential of targeting SUCNR1 in periodontitis. Metabolomics assay compared the succinate level in the subgingival plaque of patients with mild or severe periodontitis. RNAscope and Immunofluorescence assays were conducted to validate the present of SUCNR1 in both human and mouse gingival tissues. SUCNR1 KO mice were generated. Loss and gain of function of SUCNR1 in periodontitis were compared between SUCNR1 KO and WT mice. We introduced periodontitis in WT and KO mice, and then compared inflammatory markers, oral microbiota profile as well as alveolar bone loss. SUCNR1 antagonist (7a) was synthesized and its efficacy was tested by SUCNR1 activity

assay. Gel formulation of 7a was developed to assess the therapeutic effect of SUCNR1 antagonist *in-vivo*. All the reagents and software used in this study can be found in Key resources table.

Human subjects—The study was approved by the Institutional Review Board of New York University Langone Medical Center. Subject enrollment, recruitment, and eligibility screening details were reported previously (Xu et al., 2021). Subgingival plaque samples from the distal and mesial aspects of eight posterior teeth were collected by the study clinician using the stroke technique with sterile mini Gracey curettes. The classification of mild, moderate, or severe periodontal disease followed the definition given by the CDC in collaboration with the American Academy of Periodontology (CDC-AAP) (Eke et al., 2013). Mild periodontitis was defined as ≥ two interproximal sites with ≥3 mm attachment loss, and ≥2 mm interproximal sites with probing depth ≥4 mm (not on the same tooth), or one interproximal site with PD ≥5 mm. Moderate periodontitis was defined as two or more interproximal sites with ≥4 mm clinical AL (noton the same tooth), or two or more interproximal sites with PD ≥5 mm, also not on the same tooth. Severe periodontitis was defined as having two or more interproximal sites with ≥6 mm AL (not on the same tooth), and one or more interproximal site(s) with ≥5 mm PD. The samples were then placed into individual sterile 2 mL microcentrifuge tubes with transport (TE) buffer and kept on ice until delivered to the lab, where PMFS buffer and aprotinin were added, labeled, and stored at −80°C until further analysis.

Animals—All animal experiments conducted in this study were approved by Institutional Animal Care and Use Committee (IACUC) and in accordance with the Division of Laboratory Animal Resources, and the animals were housed in Specific Pathogen Free units at the New York University animal facility. All mice are C57BL/6J (B6) background unless stated otherwise. Global knockout of SUCNR1 (KO) mice were generated from EIIa-Cre (Lakso et al., 1996) (Jackson Laboratory, Bar Harbor, ME, USA) and SUCNR1 flox mice, which were created using a TurboKnockout gene targeting strategy by Cyagen and Taconic Companies. Experimental and control mice were typically housed in the same cages and the bedding of the breeders was exchanged to minimize the environmental impact.

Periodontitis models

Ligature/*F. nucleatum* model: 14-week-old male mice were anesthetized with Ketamine/Xylazine cocktail, then tied with a 6–0 silk ligature (Roboz Surgical Instrument Co., MD, USA) around the maxillary right side second molar. The ligature was kept in place for 5 days before removal. Sterile swabs were soaked in 100 μL of 2.5×10^9/mL *F. nucleatum* in PBS (Puritan, ME, USA. Catalog number: 25-806-2WA) and inoculated into mice around the ligature affected gingival tissues and stay there for 30 s. Inoculations were performed twice a week for four weeks.

Short-term ligature only model: 14-week-old male mice that were anesthetized with Ketamine/Xylazine cocktail. A 5–0 silk ligature (Roboz Surgical Instrument Co., MD, USA) was then tied around the maxillary second molar on both sides and left there for 7 days.

Mice were randomly assigned to receive 3 μL vehicle or 7a gel formulation by every other day local delivery.

Five days ligature only model: Three-month-old WT and KO male mice were anesthetized with Ketamine/Xylazine cocktail. A 6–0 silk ligature (Roboz Surgical Instrument Co., MD, USA) was then tied around the maxillary second molar on both sides and left there 5 days without other intervention. Maxillae samples were collected and proceeded to uCT analysis afterward.

LPS-P.g induced Periodontitis model: Three-month-old WT and KO female mice were anesthetized with 2–5% isoflurane through a nose cone. Thrice weekly, using a 10-μL Hamilton syringe with a 33-gauge needle, 10 μg *Porphyromonas gingivalis*-derived LPS (InvivoGen, San Diego, CA) in 2 μL sterile endotoxin-free water (InvivoGen, San Diego, CA) were injected into the gingival tissue between the right first and second maxillary molars. At the same point on the left side and using the same-sized needle, 2 μL sterile endotoxin-free water was injected as a sham treatment. Mice were randomly assigned to receive PBS or succinate (4 mM/kg) by daily intraperitoneal injection for four weeks. Mice were monitored daily to provide oral hygiene and assess healing and inflammation before being euthanized after four weeks of treatment. Serum, periodontium tissue, maxilla, mandible, and long bones from hind limbs were collected.

Bacterial culture—*F. nucleatum* (ATCC 10953) was obtained from the American Type Culture Collection (Manassas, VA, USA). *F. nucleatum* was cultivated under anaerobic conditions (80% N2, 10% CO2, 10% H2) in a Whitley A35 Anaerobic Station (Don Whitley Scientific, West Yorkshire, UK) at 37°C. For maintained growth on solid media, tryptic soy agar plates with 5% sheep blood (BD biosciences, San Jose, CA, USA) were used. For the base liquid medium, BBL brain heart infusion broth (modified) (BD biosciences, San Jose, CA, USA) was used. Filter sterilized succinate was added to the liquid base medium to a final concentration of 0, 25, 50, or 100 μM. All treatments were performed in triplicate, with 7 mL of medium in 15 mL Falcon tubes with caps loosely fashioned. An inoculation volume of 2% (vol/vol) of overnight liquid culture was used to inoculate all treatments. All liquid media was fully reduced under anaerobic conditions prior to inoculation. Colony-forming unit (CFU) measurements were performed on tryptic soy agar plates with 5% sheep blood.

Cell culture—Mouse primary osteoclast culture and TRAP staining: The bone marrow was flushed from 12-week-old mice (mixed gender) femur with cold PBS, single-cell suspension was acquired by passing the media through a syringe with a 19-gauge needle at least 5 times. After centrifugation, the cells were cultured with α-minimum Eagle's medium containing 30 ng ml^{-1} M-CSF and 50 ng mL^{-1} RANKL as previously described (Guo et al., 2017) in a 37°C, 5% (v/v) CO2, humidified incubator. TRAP staining was performed using an Acid Phosphatase Kit according to the manufacturer's instructions (Sigma, cat# 387A). Multinuclear (>10 nuclei) TRAP + cells were counted as osteoclasts using an EVOS cell imaging system (Life Technologies, Carlsbad, CA, USA).

Human Gingival Fibroblast cells (HGF-1, ATCC CRL-2014) were purchased from ATCC and maintained in Dulbecco's Modified Eagle's Medium with 10% fetal bovine serum in a 37°C, 5% (v/v) CO2, humidified incubator following the ATCC provided instruction.

METHOD DETAILS

LC-MS/MS with the hybrid metabolomics—Samples were subject to a liquid chromatography-mass spectrometry (LCMS) analysis to detect and quantify known peaks. Metabolite extraction was carried out on each sample based on previously described methods (Li et al., 2015). The LC column was a MilliporeTM ZIC-pHILIC (2.1 × 150 mm, 5 μm) coupled to a Dionex Ultimate 3000TM system, and the column oven temperature was set to 25°C for the gradient elution. A flow rate of 100 μL/min was used with the following buffers; A) 10 mM ammonium carbonate in water, pH 9.0, and B) neat acetonitrile. The gradient profile was as follows; 80–20%B (0–30 min), 20–80%B (30–31 min), 80–80%B (31–42 min). Injection volume was set to 2 μL for all analyses (42 min total run time per injection). MS analyses were carried out by coupling the LC system to a Thermo Q Exactive HFTM mass spectrometer operating in heated electrospray ionization mode (HESI). Method duration was 30 min with a polarity switching data-dependent Top 5 method for both positive and negative modes. Spray voltage for both positive and negative modes was 3.5kV, and the capillary temperature was set to 320°C with a sheath gas rate of 35, aux gas of 10, and max spray current of 100 μA. The full MS scan for both polarities utilized 120,000 resolution with an AGC target of 3×10^6 and a maximum IT of 100 ms, and the scan range was from 67–1000 m/z. Tandem MS spectra for both positive and negative mode used a resolution of 15,000, AGC target of 1×10^5, maximum IT of 50 ms, isolation window of 0.4 m/z, isolation offset of 0.1 m/z, fixed first mass of 50 m/z, and 3-way multiplexed normalized collision energies (nCE) of 10, 35, 80. The minimum AGC target was 1×10^4 with an intensity threshold of 2×10^5. All data were acquired in profile mode.

Total Bacterial DNA extraction and 16S rRNA Gene Sequencing—Total bacterial genomic DNA was purified from all samples using the QIAamp PowerFecal Kit (Qiagen). Extracted DNA was then quantified for concentration and purity initially using a NanoDrop 2000 spectrophotometer (Thermo Scientific), further verified fluoro-metrically using a Quant-iT PicoGreen dsDNA Assay Kit (Invitrogen) using the SpectraMax M5 microplate reader (Molecular Devices) and stored at −20°C until further analysis.

16S rRNA gene library preparation involved amplifying the V3-V4 hypervariable region of the 16S rRNA gene in the samples in accordance with the Illumina 16S metagenomics protocol (Part #15044223 Rev. B). Briefly, the bacterial DNA samples were diluted or concentrated to 10 ng/uL, and PCR amplified using 2x KAPA HiFi HotStart ReadyMix DNA polymerase (KapaBiosystems), primer set 341F (5′-CCTACGGGNGGCWGCAG-3′) and 805R (5′-GACTACHVGGGTATCTAATCC-3′), each with overhang adapter sequences (IDT). PCR conditions were 95°C (3 min), with 25 cycles of 9°C (30 s), 55°C (30 s), 72°C (30 s), and a final extension at 72°C (5 min). Amplicons were purified using AMPure XP beads, and a second PCR was performed with dual indices from the Nextera XT Index Kit (Illumina) and 2x KAPA HiFi HotStart ReadyMix DNA polymerase. The second PCR amplification was performed at 95°C (3 min), with 8 cycles of 95°C (30 s), 55°C (30 s),

72°C (30 s), and a final extension at 72°C (5 min) and purified with AMPure XP beads. Libraries were quantified again using the PicoGreen assay, and size was confirmed by agarose gel electrophoresis. Equimolar amounts of each sample were pooled, denatured, and sequenced using the 300-bp paired-end sequencing protocol and Illumina's MiSeq Reagent Kit V3 (600 cycles).

Sequence data in FASTQ format were demultiplexed and imported into the Quantitative Insights into Microbial Ecology pipeline v2.0 (QIIME2) and stored in Qiime2 artifact (Bolyen et al., 2019). To remove the 16S primer, do quality control and chimera checking, *dada2 denoise-paired* command was used with the following parameters: *–p-trim-left-f 17 –p-trim-left-r 21 –p-trunc-len-f 300 –p-trunc-len-r 222(Mice sample data); –p-trim-left-f 17 –p-trim-left-r 21 –p-trunc-len-f 300 –p-trunc-len-r 196* (human sample data). A phylogenetic tree was created with *qiime phylogeny align-to-tree-mafft-fasttree*. For taxonomic classification, we trained the Naive Bayes classifier on the 16S rRNA gene V3-V4 region with the primers 341F 5'-CCTACGGGNGGCWGCAG-3′ and 806R 3' – GACTACHVGGGTATC-TAATCC - 5′, and classified the representative sequences using Greengenes reference database v13.8 for mice data and Human Oral Microbiome Database: HOMD v15.2 for human data. We performed a taxa-based feature table filtering using *taxa filter-table* command to filter out the non-Bacteria taxa and Chloroplast.

QIIME2 outputs including biom tables, phylogenetic tree files, and taxonomy files were imported into R (v4.0.5) for visualization. Alpha and beta diversity were computed and plotted using the Phyloseq r package (v.1.34). Pairwise comparisons for alpha diversity indices were conducted using a Wilcoxon rank-sum test with a p value less than 0.05 considered statistically significant. Beta diversity Principal Coordinates Analysis (PCoA) plots were generated based on a Bray-Curtis dissimilarity matrix and Weighted Unifrac distance matrix, and significance between clusters was calculated with permutational multivariate analysis of variance (adonis) with vegan r package (v2.5.7). Network analysis was done using qiime make_otu_network.py script and visualized in Cytoscape (v3.8.2) (Shannon et al., 2003). Phylum-level bar-plots were generated in ggplot2 based on the phyloseq object that was agglomerated over the phylum level. Genus-level heatmaps were plotted based on the feature table collapsed at level 6 and normalized by row Z score. Differential abundant taxa between each group were identified using Wilcoxon rank-sum test. To further identify significant taxa between groups, we used the MicrobiotaProcess r package (v.1.2.2) to perform Linear discriminant analysis (LDA).

Spearman's rank correlation coefficient for comparing the relative abundance of the top 40 genera and succinate levels in samples were calculated using the Hmisc r package (v.4.5.0). Correlation-based network plot was generated in MetScape 3 (Basu et al., 2017) for Cytoscape (v. 3.8.2).

Succinate colorimetric assay—Mice blood was collected through cardiac puncture and placed in BD microtainer serum separator at room temperature for at least 30 minutes, followed by 10 min centrifugation at 200g to allow the serum to separate. Serum samples were aliquoted upon separation and flash froze till use. Assay was performed following manufacturer's protocol.

Immunohistochemistry—Human gingival tissue samples were collected as surgical waste from clinics using NYU School of Medicine IRB approved protocol (Pushalkar et al., 2014). Samples were preserved in 10% neutral buffered formalin, followed by dehydration and then embedded in paraffin. The paraffin block was sectioned at 5 μm thickness. Sections were deparaffinized and stained on a Leica BondRX autostainer, according to the manufacturers' instructions. In brief, sections underwent epitope retrieval for 20 min at 100°C with Leica Biosystems ER1 solution (pH 6.0, AR9961) followed by a 30 min incubation at 22°C with anti-GPR91 (Abcam, Cambridge, United Kingdom) diluted 1:200 in Leica diluent (Leica, Cat ARD1001EA) and subsequent detection using the BOND Polymer Refine Detection System (Leica, DS9800). Sections were counter-stained with hematoxylin scanned on a Hamamatsu Nanozoomer HT whole slide scanner and imported into the NYU Omero image database for viewing and annotation.

Immunofluorescence—Maxillae were fixed in 10% buffered formalin for 48 h, followed by 4 weeks decalcification in 10% EDTA. EDTA decalcification solution was changed freshly every other day. The decalcified maxillae tissue was then processed through graded ethanols, xylene and into paraffin in a Leica Peloris automated processor., The paraffin blocks were sectioned parallel to the sagittal axis of the maxillae at 5 μm thickness using Leica Rm2135 rotary microtone. After deparaffinization and rehydration, tissue slides were washed with PBS 3 times then blocked in blocking solution for 1 h at room temperature. Next, the slides were incubated with 1:100 blocking solution diluted SUCNR1 primary antibody (Novus Biologicals, Littleton, CO, USA) at 4°C overnight. After 3 times washing with PBS, the slides were incubated with Alexa Fluor 488 conjugated secondary antibody (Cell Signaling Technology, Danvers, MA, USA) for 1 h at room temperature, followed by 4′,6-diamidino-2-phenylindole (DAPI) counterstaining for nucleus indication. The fluorescence microscopy images were captured using the Nikon Eclipse E600 system (Nikon, Tokyo, Japan).

HGF-1 cells were seeded at 10,000 cells/well in Millicell EZ 8-well glass chamber slide. After 48 h, culture medium was removed and cells were fixed with 10% buffered formalin for 30 min, triple washed with PBS and then proceed with immunostaining described above. Cell structure was stained with F-actin probe ActinGreen 488 ReadyProbes Reagent.

In-situ hybridization (RNAScope)—Animal was perfused with Diethyl pyrocarbonate (DEPC) treated 4% paraformaldehyde (PFA), and gingival tissue was then immersed in 4% PFA overnight before proceeding to automated tissue processing and paraffin embedding. The gingival paraffin block was sectioned at 4–5 μm thickness using Leica Rm2235 rotary microtone. RNA *in situ* hybridization (RNA_ISH) was performed in accordance with RNAscope LS multiplex Fluorescent assay protocols USM#322800 (Advanced Cell Diagnostics, Hayward, CA, USA) on Leica Bond Rx Automated System. The slide was baked and dewaxed in the automated system, the target was retrieved using epitope retrieval buffer 2, pH9 at 95°C for 15 min, and the sample slide was stained with RNAscope 2.5 LS Probe - Mm-Sucnr1-C3 and DAPI (Advanced Cell Diagnostics, Hayward, CA, USA), followed by wheat germ agglutinin or WGA (Thermo Fisher #W849). After staining, the slide was mounted with Prolong Gold Antifade mountant (Invitrogen) and scanned using

MoTiF Vectra Polaris 3.0 (Akoya Biosciences, Marlborough, MA, USA) Whole Slide Multispectral Imaging System at 20× magnification. The slide was viewed with Phenochart Viewer and analyzed using InForm Machine Learning software. Figures were imported by Omero Insight and finalized using Omero Figure.

Three-dimensional micro-computed tomography analysis—Maxillae were fixed in 10% buffered formalin for 48 h, washed with PBS, and placed in a standardized sample holder. The microcomputed tomography (μCT) of the maxillae were scanned at settings of 60 kV, 167 μA, and a spatial resolution of 9.7 μm using a SkyScan 1172 high-resolution scanner (Bruker microCT, Kontich, Antwerp, Belgium). Reconstruction was conducted using NRecon at a 9.7-μm pixel size. The original maxillae data after reconstruction were imported into the DataViewer for reorientation. The sagittal plane crossed both the third root of the first maxillary molar and the first root of the second maxillary molar was captured in the transaxial image. The distance between cementoenamel junctions (CEJ) to the alveolar bone (AB) crest was measured in ImageJ, and the 3D image of the one side maxillae was generated using CTVox.

TRAP staining—Maxillae paraffin blocks were prepared as previously described. Five-micron paraffin-embedded sections were cut parallel to the sagittal axis of the maxillae from three distinct levels. In brief, continuous sectioning was performed on each sample, and 3 tissue sections 25 um apart from each other were picked onto the slides for TRAP staining. The slides were baked and dewaxed, followed by the TRAP staining. The basal medium for the TRAP staining was prepared by adding 110 mM Sodium acetate, 50 mM L-(+) Tartaric acid, and 50 mM Glacial acetic acid to water, and pH was adjusted to 4.8 using sodium hydroxide. The complete solution was prepared by freshly adding 0.01% Napthol AS-MX Phosphate and 0.06% Fast Red Violet LB salt into the basal medium. Slides were incubated in the complete TRAP staining solution at 37°C for 60 min then rinsed in distilled water, followed by counterstaining with 0.08% fast green for 1 min. TRAP + cells on alveolar bone area were counted as osteoclasts using an EVOS cell imaging system, alveolar bone areas were measured using ImageJ. The average number of TRAP + cells from 3 sections of different level were calculated to represent each samples' TRAP + cell number per alveolar bone area.

Cytokine measurement in mice serum—We determined the serum TNF-α and IL-1β levels using Quantikine ELISA Kits from R&D Systems (Catalog number: MTA00B and MLB00C) following the instructions provided by the manufacturers.We used V-PLEX Proinflammatory Panel 1 Mouse Kit to examine additional inflammatory markers. In brief, mice serum collected previously were thawed and diluted 2 times using diluent 41 supplemented in the kit. Assay was performed following manufacture's instruction. After Read Buffer T was added into each well, plate was read on a MESO QuickPlex SQ 120 instrument, data was then analyzed with MSD Discovery Workbench.

Cytokine measurement in HGF-1 culture supernatant—HGF-1 cells were seeded at 20,000 cells/well in two tissue culture treated 96 well plates. After 48 h, culture medium was refreshed with fresh complete medium described previously for one of the plate, and 7a was

given into the culture media 15 min prior to the LPS treatment. 4 h later, same treatment and procedure was performed with the other plate. In another 4 h, supernatant from two plates were collected and loaded into the V-PLEX Plus Proinflammatory Panel 1 Human Kit freshly without any frozen and thaw cycle. Assay was performed following manufacture's instruction. After Read Buffer T was added into each well, plate was read on a MESO QuickPlex SQ 120 instrument, data was then analyzed with MSD Discovery Workbench.

Compound 7a synthesis and gel formulation—All reagents/solvents were used as received from commercial suppliers unless otherwise noted. Reactions were conducted in screwcap glass vials with Teflon-lined caps/round bottom flasks. Reactions were monitored by thin-layer chromatography (TLC) using a TLC silica gel 60 F254 glass plate. Compounds were detected by UV (254 nm) or staining (ninhydrin or phosphomolybdic acid). Column chromatography was performed using 230–400 mesh silica gel in all cases unless otherwise mentioned.

Nuclear magnetic resonance (^{1}H NMR, ^{13}C NMR) experiments were performed on Bruker Avance 400, 500, or 600 MHz NMR spectrometer and are referenced to the solvent resonances. Chemical shifts (δ) are reported in parts per million (ppm), and coupling constants (J) were expressed in hertz (Hz). Standard Abbreviations are used to designate resonance multiplicities. For formulations study, the polymers PLGA (0.26–0.54 dL/g), PLGA (0.55–0.75 dL/g in HFIP), Poly (D, L-lactide)-ester terminated (0.55–0.75 dL/g in CHCCl3), poly (ε-caprolactone)-ester terminated, (0.65–0.85 dL/g in CHCCl3) were purchased from Lactel Absorbable Polymers. The specified amount of polymer was dissolved in 4 mL of the solvent system. An appropriate quantity of compound-7a (at a final concentration of 5.0 mg/mL) was added to the polymeric solution and mixed by vortexing until complete dissolution.

***In vitro* SUCNR1 activity assay—**Human Succinate Receptor 1 Ready –to-Assay Cell kit was used to assess the activity of SUCNR1 upon activation by ligand (succinate 500 μM) in the presence or absence of antagonists. Screen Quest Fluo-8 No Wash Calcium Assay Kit was used to detect the signal per manufacture's protocol. Cells were seeded at 5,000 cells/well in a black plate clear bottom 96 well assay plate for 24h in the growth medium included from the cell kit before the calcium dye was added. Forty-five minutes later, the antagonists were added at indicated concentrations. Fifteen minutes later, the ligand was added, and the fluorescent signal (EX/EM: 485/525) was measured immediately on a plate reader.

Quantification of gene expression—Gingival tissue around the ligature site was taken out and snap-frozen with liquid nitrogen at the time of dissection and stored at −80°C until RNA extraction. Total RNA was isolated using TRIzol Reagent, and it was purified using the RNeasy kit (Qiagen, Hilden, Germany). Following TaqMan reverse transcription, polymerase chain reaction (PCR) was performed in a BioRad 384-module using an SYBR Green (Applied Biosystems, Foster City, CA) method with primers for the indicated genes (Table S1).*F. nucleatum* was cultured and treated with PBS or 100 μM succinate as described above. *F. nucleatum* pellets were obtained by spinning at 3000 rpm for 5 min. Culture medium was discarded and TRIzol was added to the pellet, followed by the RNA

extraction, reverse transcription and polymerase chain reaction (PCR) mentioned previously. 16S was used as internal control and other interested genes were measured as listed in Table S1.

Bacteroidetes composition in ligature samples was determined by real-time PCR using *Bacteroidetes* and total bacteria primers. The assay was performed in a 10 μL reaction system contained 2× Power SYBR Green master mix (Applied Biosystems), 100 nmol L^{-1} of forward and reverse primers, and 10 ng sample DNA on a Bio-Rad CFX384 real-time system. The reaction was programmed as follows: denaturation at 94°C for 10 min, 40 cycles of 94°C for 1 min, annealing at 60°C for 1 min, and elongation at 72°C for 90 s, followed by a final elongation at 72°C for 5 min. Total Bacterial DNA extracted from pure *E.coli* culture was used to plot a standard curve to calculate bacterial DNA concentration in each sample.

QUANTIFICATION AND STATISTICAL ANALYSIS

16S rRNA Gene Sequencing data analysis has been described in Method details above. All other data figures were analyzed and generated by GraphPad Prism 9.1.1. Figures 1A, 1B, 5C, 5F-5J, S1B, S1C, S2B, S4B-S4E, and S5B were analyzed using Student's t-test. Figures 2D-2I, 3G, 4E-4G, S2C-S2F, and S3B were analyzed using ANOVA with the Tukey's post hoc test. Figures 3C and 4C were analyzed using ANOVA with the Dunnett's post hoc test. Bars in figures represent the mean ± SEM unless stated otherwise.

Supplementary Material

Refer to Web version on PubMed Central for supplementary material.

ACKNOWLEDGMENTS

This work was supported by NIH grants DE027074 (to X.L., D.S., and D.T.G.), DE028212 and AG068857 (to X.L. and D.S.), and R01DE017732 (to D.T.G.). We thank the NYU CSCB Micro CT Core and Metabolomics Laboratory Core Facility for equipment support. We also thank members of the Experimental Pathology Research Laboratory, which is partially supported by Cancer Center Support Grant P30CA016087 at NYU Langone's Laura and Isaac Perlmutter Cancer Center.

REFERENCES

Aguiar CJ, Rocha-Franco JA, Sousa PA, Santos AK, Ladeira M, Rocha-Resende C, Ladeira LO, Resende RR, Botoni FA, Barrouin Melo M, et al. (2014). Succinate causes pathological cardiomyocyte hypertrophy through GPR91 activation. Cell Commun. Signal 12, 78. [PubMed: 25539979]

Basu S, Duren W, Evans CR, Burant CF, Michailidis G, and Karnovsky A (2017). Sparse network modeling and metscape-based visualization methods for the analysis of large-scale metabolomics data. Bioinformatics 33, 1545–1553. [PubMed: 28137712]

Bolyen E, Rideout JR, Dillon MR, Bokulich NA, Abnet CC, Al-Ghalith GA, Alexander H, Alm EJ, Arumugam M, Asnicar F, et al. (2019). Reproducible, interactive, scalable and extensible microbiome data science using QIIME 2. Nat. Biotechnol 37, 852–857. [PubMed: 31341288]

Castro SA, Collighan R, Lambert PA, Dias IH, Chauhan P, Bland CE, Milic I, Milward MR, Cooper PR, and Devitt A (2017). Porphyromonas gingivalis gingipains cause defective macrophage migration towards apoptotic cells and inhibit phagocytosis of primary apoptotic neutrophils. Cell Death Dis. 8, e2644. [PubMed: 28252646]

Ceccarani C, Foschi C, Parolin C, D'Antuono A, Gaspari V, Consolandi C, Laghi L, Camboni T, Vitali B, Severgnini M, and Marangoni A (2019). Diversity of vaginal microbiome and metabolome during genital infections. Sci. Rep 9, 14095. [PubMed: 31575935]

Chouchani ET, Pell VR, Gaude E, Aksentijević D, Sundier SY, Robb EL, Logan A, Nadtochiy SM, Ord ENJ, Smith AC, et al. (2014). Ischaemic accumulation of succinate controls reperfusion injury through mitochondrial ROS. Nature 515, 431–435. [PubMed: 25383517]

Corrêa JD, Fernandes GR, Calderaro DC, Mendonca SMS, Silva JM, Albiero ML, Cunha FQ, Xiao E, Ferreira GA, Teixeira AL, et al. (2019). Oral microbial dysbiosis linked to worsened periodontal condition in rheumatoid arthritis patients. Sci. Rep 9, 8379. [PubMed: 31182740]

Curtis MA, Diaz PI, and Van Dyke TE (2020). The role of the microbiota in periodontal disease. Periodontol. 2000 83, 14–25.

De Vadder F, Kovatcheva-Datchary P, Zitoun C, Duchampt A, Bäckhed F , and Mithieux G (2016). Microbiota-produced succinate improves glucose homeostasis via intestinal gluconeogenesis. Cell Metab. 24, 151–157. [PubMed: 27411015]

Ebersole JL, Kesavalu L, Schneider SL, Machen RL, and Holt SC (1995). Comparative virulence of periodontopathogens in a mouse abscess model. Oral Dis. 1, 115–128. [PubMed: 8705817]

Eke PI, Dye BA, Wei L, Slade GD, Thornton-Evans GO, Beck JD, Taylor GW, Borgnakke WS, Page RC, and Genco RJ (2013). Self-reported measures for surveillance of periodontitis. J. Dent. Res 92, 1041–1047. [PubMed: 24065636]

Eke PI, Dye BA, Wei L, Slade GD, Thornton-Evans GO, Borgnakke WS, Taylor GW, Page RC, Beck JD, and Genco RJ (2015). Update on prevalence of periodontitis in adults in the United States: NHANES 2009 to 2012. J. Periodontol 86, 611–622. [PubMed: 25688694]

Ferreyra JA, Wu KJ, Hryckowian AJ, Bouley DM, Weimer BC, and Sonnenburg JL (2014). Gut microbiota-produced succinate promotes C. difficile infection after antibiotic treatment or motility disturbance. Cell Host Microbe 16, 770–777. [PubMed: 25498344]

Foster JS, and Kolenbrander PE (2004). Development of a multispecies oral bacterial community in a saliva-conditioned flow cell. Appl. Environ. Microbiol 70, 4340–4348. [PubMed: 15240317]

Fukui S, Shimoyama T, Tamura K, Yamamura M, and Satomi M (1997). Mucosal blood flow and generation of superoxide in rat experimental colitis induced by succinic acid. J. Gastroenterol 32, 464–471. [PubMed: 9250892]

Ganther S, Radaic A, Malone E, Kamarajan P, Chang NYN, Tafolla C, Zhan L, Fenno JC, and Kapila YL (2021). Treponema denticola dentilisin triggered TLR2/MyD88 activation upregulates a tissue destructive program involving MMPs via Sp1 in human oral cells. PLoS Pathog. 17, e1009311. [PubMed: 34255809]

Graves DT, Ding Z, and Yang Y (2020). The impact of diabetes on periodontal diseases. Periodontol. 2000 82, 214–224.

Graves DT, Liu R, and Oates TW (2007). Diabetes-enhanced inflammation and apoptosis: impact on periodontal pathosis. Periodontol. 2000 45, 128–137.

Grenier D (1992). Demonstration of a bimodal coaggregation reaction between Porphyromonas gingivalis and Treponema denticola. Oral Microbiol. Immunol 7, 280–284. [PubMed: 1337373]

Grenier D, and Mayrand D (1986). Nutritional relationships between oral bacteria. Infect. Immun 53, 616–620. [PubMed: 2875029]

Guo Y, Cho SW, Saxena D, and Li X (2020). Multifaceted actions of succinate as a signaling transmitter vary with its cellular locations. Endocrinol. Metab 35, 36–43.

Guo Y, Xie C, Li X, Yang J, Yu T, Zhang R, Zhang T, Saxena D, Snyder M, Wu Y, and Li X (2017). Succinate and its G-protein-coupled receptor stimulates osteoclastogenesis. Nat. Commun 8, 15621. [PubMed: 28561074]

Hajishengallis G (2015). Periodontitis: from microbial immune subversion to systemic inflammation. Nat. Rev. Immunol 15, 30–44. [PubMed: 25534621]

Hajishengallis G, and Chavakis T (2021). Local and systemic mechanisms linking periodontal disease and inflammatory comorbidities. Nat. Rev. Immunol 21, 426–440. [PubMed: 33510490]

He W, Miao FJP, Lin DCH, Schwandner RT, Wang Z, Gao J, Chen J-L, Tian H, and Ling L (2004). Citric acid cycle intermediates as ligands for orphan G-protein-coupled receptors. Nature 429, 188–193. [PubMed: 15141213]

Hedberg ME, Moore ERB, Svensson-Stadler L, Hörstedt P, Baranov V, Hernell O, Wai SN, Hammarström S, and Hammarström ML (2012). Lachnoanaerobaculum gen. nov., a new genus in the Lachnospiraceae: characterization of Lachnoanaerobaculum umeaense gen. nov., sp. nov., isolated from the human small intestine, and Lachnoanaerobaculum orale sp. nov., isolated from saliva, and reclassification of Eubacterium saburreum (Prevot 1966) Holdeman and Moore 1970 as Lachnoanaerobaculum saburreum comb. nov. Int. J. Syst. Evol. Microbiol 62, 2685–2690. [PubMed: 22228654]

Hoare A, Soto C, Rojas-Celis V, and Bravo D (2019). Chronic inflammation as a link between periodontitis and carcinogenesis. Mediators Inflamm. 2079, 1029857.

Janssen PH (1992). Growth yield increase and ATP formation linked to succinate decarboxylation in Veillonella parvula. Arch. Microbiol 157, 442–445. [PubMed: 1510569]

Kassem A, Henning P, Lundberg P, Souza PPC, Lindholm C, and Lerner UH (2015). Porphyromonas gingivalis stimulates bone resorption by enhancing RANKL (receptor activator of NF-kappaB ligand) through activation of toll-like receptor 2 in osteoblasts. J. Biol. Chem 290, 20147–20158. [PubMed: 26085099]

Kilian M, Chapple ILC, Hannig M, Marsh PD, Meuric V, Pedersen AML, Tonetti MS, Wade WG, and Zaura E (2016). The oral microbiome - an update for oral healthcare professionals. Br. Dent. J 221, 657–666. [PubMed: 27857087]

Krebs HA (1970). Rate control of the tricarboxylic acid cycle. Adv. Enzyme Regul 8, 335–353. [PubMed: 4920378]

Lakso M, Pichel JG, Gorman JR, Sauer B, Okamoto Y, Lee E, Alt FW, and Westphal H (1996). Efficient in vivo manipulation of mouse genomic sequences at the zygote stage. Proc. Natl. Acad. Sci. USA 93, 5860–5865. [PubMed: 8650183]

Lamont RJ, Koo H, and Hajishengallis G (2018). The oral microbiota: dynamic communities and host interactions. Nat. Rev. Microbiol 16, 745–759. [PubMed: 30301974]

Lewis GD, Farrell L, Wood MJ, Martinovic M, Arany Z, Rowe GC, Souza A, Cheng S, McCabe EL, Yang E, et al. (2010). Metabolic signatures of exercise in human plasma. Sci. Transl. Med 2, 33ra37.

Li X, Guo Y, Yan W, Snyder MP, and Li X (2015). Metformin improves diabetic bone health by Re-balancing catabolism and nitrogen disposal. PLoS One 10, e0146152. [PubMed: 26716870]

Lim R, and Lappas M (2020). Inhibition of GPR91 reduces inflammatory mediators involved in active labor in myometrium. Mediators Inflamm. 2020, 6454282. [PubMed: 32377163]

Littlewood-Evans A, Sarret S, Apfel V, Loesle P, Dawson J, Zhang J, Muller A, Tigani B, Kneuer R, Patel S, et al. (2016). GPR91 senses extracellular succinate released from inflammatory macrophages and exacerbates rheumatoid arthritis. J. Exp. Med 213, 1655–1662. [PubMed: 27481132]

Lu R, Meng H, Gao X, Xu L, and Feng X (2014). Effect of non-surgical periodontal treatment on short chain fatty acid levels in gingival crevicular fluid of patients with generalized aggressive periodontitis. J. Periodontal. Res 49, 574–583. [PubMed: 25340203]

Lu RF, Feng XH, Xu L, and Meng HX (2015). [Clinical and putative periodontal pathogens' features of different sites with probing depth reduction after non-surgical periodontal treatment of patients with aggressive periodontitis]. Beijing Da Xue Xue Bao Yi Xue Ban 47, 13–18. [PubMed: 25686322]

Marttila E, Järvensivu A, Sorsa T, Grenier D, Richardson M, Kari K, Tervahartiala T, and Rautemaa R (2014). Intracellular localization of Treponema denticola chymotrypsin-like proteinase in chronic periodontitis. J. Oral Microbiol 6, 24349.

McDonald NC, and White RL (2019). Reduction of fumarate to succinate mediated by Fusobacterium varium. Appl. Biochem. Biotechnol 187, 163–175. [PubMed: 29911265]

Mcllvanna E, Linden GJ, Craig SG, Lundy FT, and James JA (2021). Fusobacterium nucleatum and oral cancer: a critical review. BMC Cancer 21, 1212. [PubMed: 34774023]

Mills E, and O'Neill LAJ (2014). Succinate: a metabolic signal in inflammation. Trends Cell Biol. 24, 313–320. [PubMed: 24361092]

Mills EL, Kelly B, Logan A, Costa ASH, Varma M, Bryant CE, Tourlomousis P, Däbritz JHM, Gottlieb E, Latorre I, et al. (2016). Succinate dehydrogenase supports metabolic repurposing of mitochondria to drive inflammatory macrophages. Cell 167, 457–470.e13. [PubMed: 27667687]

Nazir MA (2017). Prevalence of periodontal disease, its association with systemic diseases and prevention. Int. J. Health Sci 11, 72–80.

Niederman R, Buyle-Bodin Y, Lu BY, Robinson P, and Naleway C (1997). Short-chain carboxylic acid concentration in human gingival crevicular fluid. J. Dent. Res 76, 575–579. [PubMed: 9042080]

Ohwaki K (1988). [High carboxylic acid level in the gingival crevicular fluid (GCF) of the patients with advanced periodontal disease]. Nihon Shishubyo Gakkai Kaishi 30, 985–995. [PubMed: 3078007]

Olsen I, and Yamazaki K (2019). Can oral bacteria affect the microbiome of the gut? J. Oral Microbiol 11, 1586422. [PubMed: 30911359]

Park J, Shokeen B, Haake SK, and Lux R (2016). Characterization of Fusobacterium nucleatum ATCC 23726 adhesins involved in strain-specific attachment to Porphyromonas gingivalis. Int. J. Oral Sci 8, 138–144.

Pushalkar S, Li X, Kurago Z, Ramanathapuram LV, Matsumura S, Fleisher KE, Glickman R, Yan W, Li Y, and Saxena D (2014). Oral microbiota and host innate immune response in bisphosphonate-related osteonecrosis of the jaw. Int. J. Oral Sci 6, 219–226. [PubMed: 25105817]

Qiqiang L, Huanxin M, and Xuejun G (2012). Longitudinal study of volatile fatty acids in the gingival crevicular fluid of patients with periodontitis before and after nonsurgical therapy. J. Periodontal. Res 47, 740–749. [PubMed: 22594616]

Rabe P, Liebing AD, Krumbholz P, Kraft R, and Stäubert C (2022). Succinate receptor 1 inhibits mitochondrial respiration in cancer cells addicted to glutamine. Cancer Lett. 526, 91–102. [PubMed: 34813893]

Rosen G, Naor R, Rahamim E, Yishai R, and Sela MN (1995). Proteases of Treponema denticola outer sheath and extracellular vesicles. Infect. Immun 63, 3973–3979. [PubMed: 7558307]

Rubić-Schneider T, Carballido-Perrig N, Regairaz C, Raad L, Jost S, Rauld C, Christen B, Wieczorek G, Kreutzer R, Dawson J, et al. (2017). GPR91 deficiency exacerbates allergic contact dermatitis while reducing arthritic disease in mice. Allergy 72, 444–452. [PubMed: 27527650]

Sadagopan N, Li W, Roberds SL, Major T, Preston GM, Yu Y, and Tones MA (2007). Circulating succinate is elevated in rodent models of hypertension and metabolic disease. Am. J. Hypertens 20, 1209–1215. [PubMed: 17954369]

Serena C, Ceperuelo-Mallafré V, Keiran N, Queipo-Orturño MI, Bernal R, Gomez-Huelgas R, Urpi-Sarda M, Sabater M, Pérez-Brocal V, Andrés-Lacueva C, et al. (2018). Elevated circulating levels of succinate in human obesity are linked to specific gut microbiota. ISME J. 12, 1642–1657. [PubMed: 29434314]

Shannon P, Markiel A, Ozier O, Baliga NS, Wang JT, Ramage D, Amin N, Schwikowski B, and Ideker T (2003). Cytoscape: a software environment for integrated models of biomolecular interaction networks. Genome Res. 13, 2498–2504. [PubMed: 14597658]

Socransky SS, Haffajee AD, Cugini MA, Smith C, and Kent RL Jr. (1998). Microbial complexes in subgingival plaque. J. Clin. Periodontol 25, 134–144. [PubMed: 9495612]

Su W, Shi J, Zhao Y, Yan F, Lei L, and Li H (2020). Porphyromonas gingivalis triggers inflammatory responses in periodontal ligament cells by succinate-succinate dehydrogenase–HIF–1α axis. Biochem. Biophys. Res. Commun 522, 184–190. [PubMed: 31757417]

Suárez LJ, Garzón H, Arboleda S, and Rodríguez A (2020). Oral dysbiosis and autoimmunity: from local periodontal responses to an imbalanced systemic immunity. A review. Front. Immunol 11, 591255. [PubMed: 33363538]

Takahashi N, and Yamada T (2000). Glucose metabolism by Prevotella intermedia and Prevotella nigrescens. Oral Microbiol. Immunol 15, 188–195. [PubMed: 11154402]

Tan KH, Seers CA, Dashper SG, Mitchell HL, Pyke JS, Meuric V, Slakeski N, Cleal SM, Chambers JL, McConville MJ, and Reynolds EC (2014). Porphyromonas gingivalis and Treponema denticola exhibit metabolic symbioses. PLoS Pathog. 10, e1003955. [PubMed: 24603978]

Tannahill GM, Curtis AM, Adamik J, Palsson-McDermott EM, McGettrick AF, Goel G, Frezza C, Bernard NJ, Kelly B, Foley NH, et al. (2013). Succinate is an inflammatory signal that induces IL-1beta through HIF-1alpha. Nature 496, 238–242. [PubMed: 23535595]

Thurnheer T, Karygianni L, Flury M, and Belibasakis GN (2019). Fusobacterium species and subspecies differentially affect the composition and architecture of supra- and subgingival biofilms models. Front. Microbiol 10, 1716. [PubMed: 31417514]

Toma I, Kang JJ, Sipos A, Vargas S, Bansal E, Hanner F, Meer E, and Peti-Peterdi J (2008). Succinate receptor GPR91 provides a direct link between high glucose levels and renin release in murine and rabbit kidney. J. Clin. Invest 118, 2526–2534. [PubMed: 18535668]

Xiao E, Mattos M, Vieira GHA, Chen S, Corrêa JD, Wu Y, Albiero ML, Bittinger K, and Graves DT (2017). Diabetes enhances IL-17 expression and alters the oral microbiome to increase its pathogenicity. Cell Host Microbe 22, 120–128.e4. [PubMed: 28704648]

Xu F, Aboseria E, Janal MN, Pushalkar S, Bederoff MV, Vasconcelos R, Sapru S, Paul B, Queiroz E, Makwana S, et al. (2021). Comparative effects of E-cigarette aerosol on periodontium of periodontitis patients. Front. Oral Health 2, 729144. 10.1101/2021.1101.1121.21250255. [PubMed: 35048050]

Yamada M, Ikegami A, and Kuramitsu HK (2005). Synergistic biofilm formation by Treponema denticola and Porphyromonas gingivalis. FEMS Microbiol. Lett 250, 271–277. [PubMed: 16085371]

Yip S, Dehcheshmeh MM, McLelland DJ, Boardman WSJ, Saputra S, Ebrahimie E, Weyrich LS, Bird PS, and Trott DJ (2021). Porphyromonas spp., Fusobacterium spp., and Bacteroides spp. dominate microbiota in the course of macropod progressive periodontal disease. Sci. Rep 11, 17775. [PubMed: 34493783]

Zaura E, Keijser BJF, Huse SM, and Crielaard W (2009). Defining the healthy "core microbiome" of oral microbial communities. BMC Microbiol. 9, 259. [PubMed: 20003481]

Highlights

- Elevation of succinate accelerates periodontitis progression
- Succinate promotes dysbiosis, inflammation, and bone loss through SUCNR1
- An antagonist is developed to suppress activation of SUCNR1
- Topical application of the SUCNR1 antagonist impedes manifestation of periodontitis

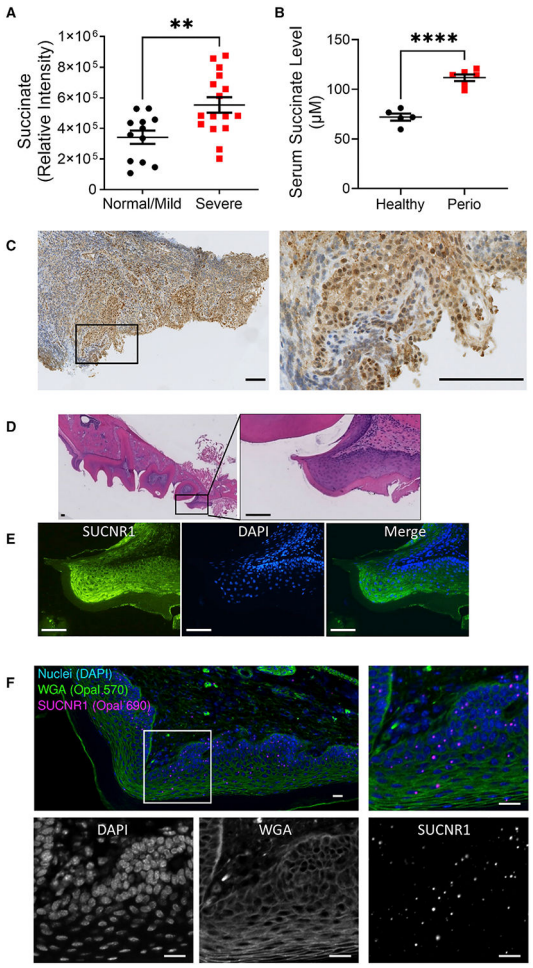

Figure 1. SUCNR1 presenting in periodontium in humans and mice

(A) Succinate levels measured by metabolomics in a cohort of individuals with or without severe periodontitis. Error bars show mean ± SEM. Normal/mild, N = 12; severe, N = 16; **p < 0.01.

(B) Succinate levels measured by colorimetric assay using serum samples from mice with or without periodontitis. Error bars show mean ± SEM. Healthy, N = 5; perio, N = 6; ****p < 0.0001).

(C) Immunohistochemistry staining of human SUCNR1 (brown) in human gingival tissue (scale bar, 100 μm).

(D and E) Histology of mouse gingiva sections with (D) H&E staining (scale bar, 100 μm) and (E) immunofluorescent staining (scale bar, 100 μm) of SUCNR1 (green) and DAPI stained nuclei (blue) in stratified squamous epithelial cells.

(F) RNAScope staining of SUCNR1 (magenta), wheat germ agglutinin (WGA)-stained cell surface (green), and DAPI stained nuclei (blue) in gingival tissue (scale bar, 20 μm).

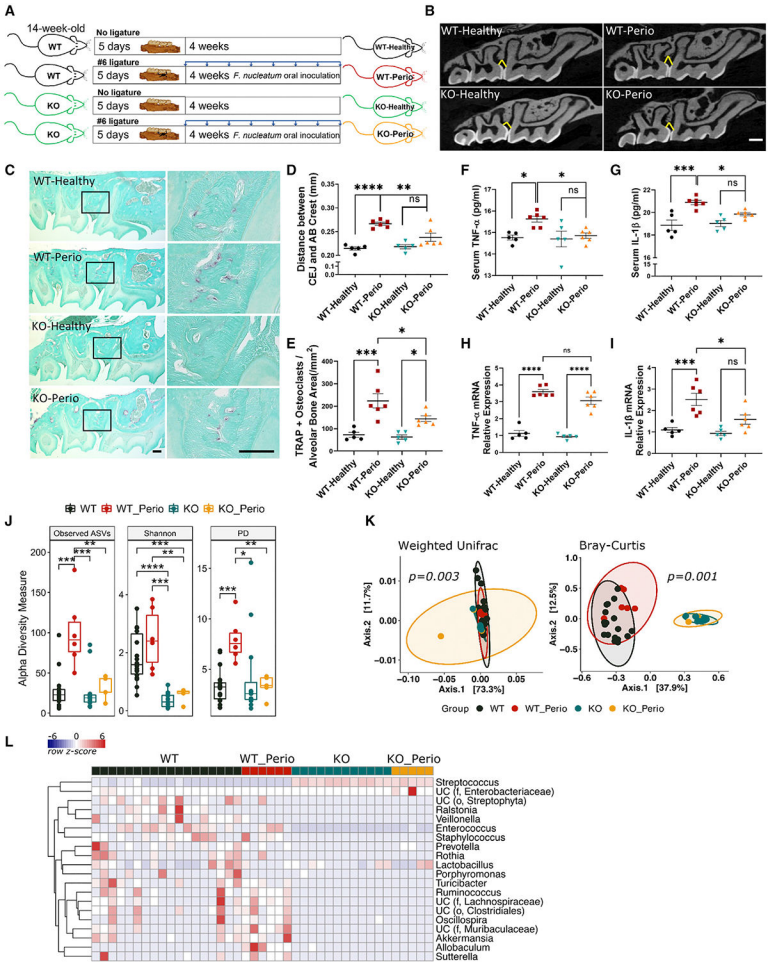

Figure 2. SUCNR1 KO mice are resistant to bone loss, inflammation, and dysbiosis induced by periodontitis

(A) Diagram of the experimental model and treatment groups.

(B and C) Representative images of (B) microcomputed tomography (μCT) of maxillae from each group (scale bar, 500 μm) and (C) Tartrate-resistant acid phosphatase (TRAP) staining on maxilla sections (scale bar, 200 μm).

(D) Quantitative μCT results. Error bars show mean ± SEM. n = 5–6, **p < 0.01, ****p < 0.0001.

(E) Quantitative results of TRAP+ cell numbers normalized by alveolar bone area from each group. Error bars show mean ± SEM. n = 5–6, *p < 0.05, ***p < 0.005.

(F and G) TNF-α (F) and IL-1β (G) protein levels in the serum of each group. Error bars show mean ± SEM. n = 5–6, *p < 0.05, ***p < 0.005.

(H and I) TNF-α (H) and IL-1β (I) relative expression in the gingival tissue of each group. Error bars show mean ± SEM. n = 5–6, *p < 0.05, ***p < 0.005, ****p < 0.0001.

(J) Alpha diversity measured by the observed number of amplicon sequence variants (ASVs), the Shannon index, and phylogenetic diversity index for swab samples from WT mice, WT mice with periodontitis (WT_perio), KO mice, and KO mice with periodontitis (KO_perio).

(K) Principal coordinates analysis (PCoA) plots for beta diversity based on the weighted UniFrac distance matrix ($p < 0.003$) and Bray-Curtis dissimilarity matrix ($p < 0.001$) showed that WT mice and KO mice clustered separately from each other.
(L) Heatmap for the top 20 genera based on relative abundance normalized by row Z score. UC, unclassified genus. The higher taxon was added to the genus name when it was unclassified.

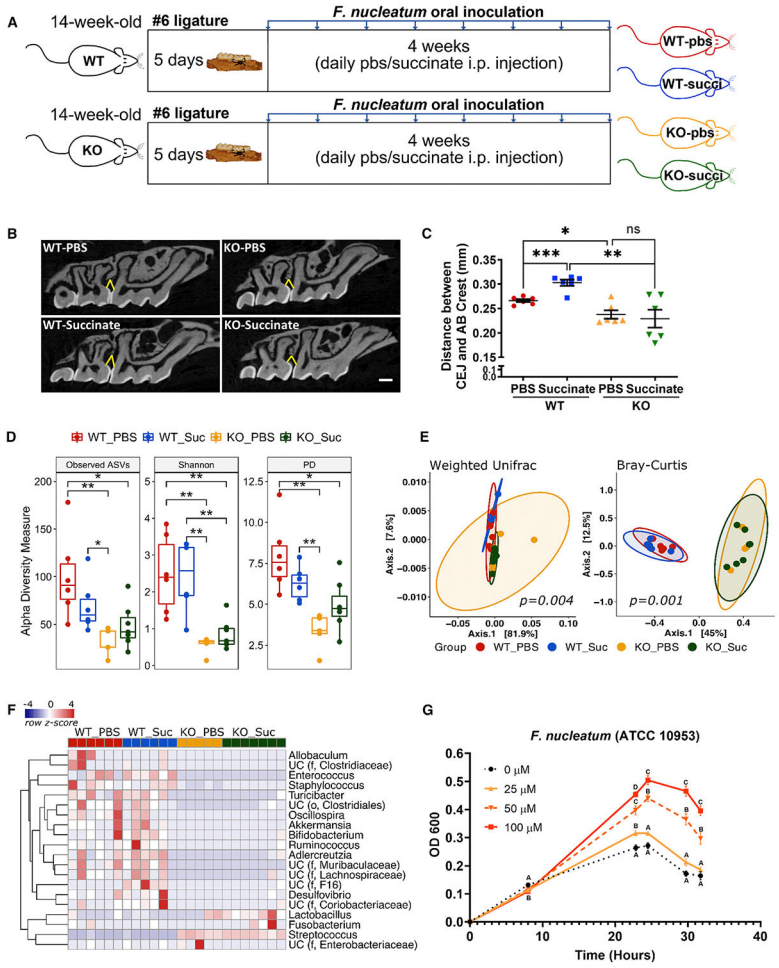

Figure 3. Succinate stimulates the pathogenesis of periodontitis

(A) Experimental design.

(B and C) Representative μCT images (B; scale bar, 500 μm) and quantitative results (C) of maxillae from each group. Error bars show mean ± SEM. n = 6, *p < 0.05, **p < 0.01, ***p < 0.005.

(D) Alpha diversity measured by the observed number of ASVs, Shannon index, and phylogenetic diversity index for swab samples from WT mice treated with PBS (WT_PBS), WT mice treated with succinate at 4 mM/kg through daily intraperitoneal injection (WT_Suc), KO mice treated with PBS (KO_PBS), and KO mice treated with succinate (KO_Suc).

(E) PCoA plots for beta diversity based on the weighted UniFrac distance matrix (p = 0.004) and Bray-Curtis dissimilarity matrix (p = 0.001) show that the groups differed in microbial community structure.

(F) Heatmap for the top 20 genera based on relative abundance normalized by row *Z* score. The higher taxon was added to the genus name when it was unclassified.

(G) Succinate stimulates growth of *F. nucleatum*. Bacterial growth is shown as optical density 600 (OD_{600}) measures over time (n = 3, SEM). Colors indicate succinate concentrations. When different letters are shown at a time point, they are statistically different from one another (ANOVA, p < 0.05 by post-hoc Tukey's test).

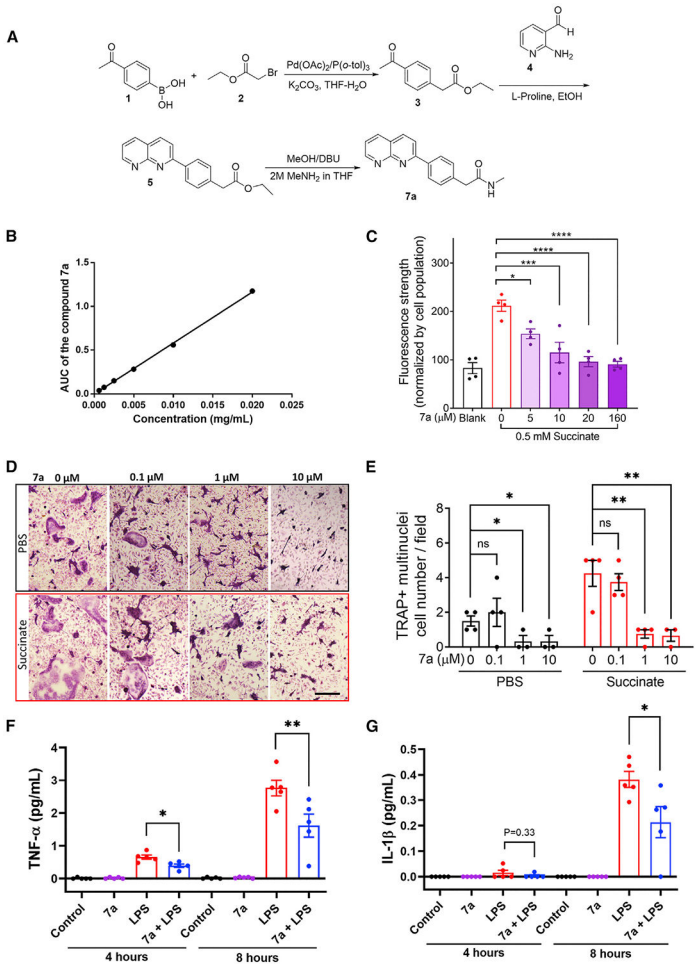

Figure 4. Development of a specific antagonist of SUCNR1 and its effects *in vitro*

(A) Schematic indicating the synthesis of compound 7a.

(B) Calibration curve of cpd-7a by UV-visible (UV-vis). The absorbance of compound 7a in various concentrations was plotted against the concentration to generate the calibration curve with a goodness of fit value of 0.9993.

(C) Efficacy of 7a in blocking activation of SUCNR1 by 0.5 mM succinate at the indicated concentrations in a reporter cell line. Error bars show mean ± SEM. n = 4, *p < 0.05, ***p < 0.005, ****p < 0.0001.

(D and E) Representative images (D; scale bar, 150 μm) and quantitative results (E) of multinucleated (nucleus number ≥ 10) TRAP+ primary osteoclast cultures with TRAP staining. Error bars show mean ± SEM. n = 4, *p < 0.05, **p < 0.01.

(F and G) TNF-α (F) and IL-1β (G) protein levels in conditioned medium of HGF1 cells treated with LPS (5 μg/mL) for 4 and 8 h in the presence or absence of 7a (50 μM) pretreatment for 15 min as indicated. Error bars show mean ± SEM. n = 5, *p < 0.05, **p < 0.01.

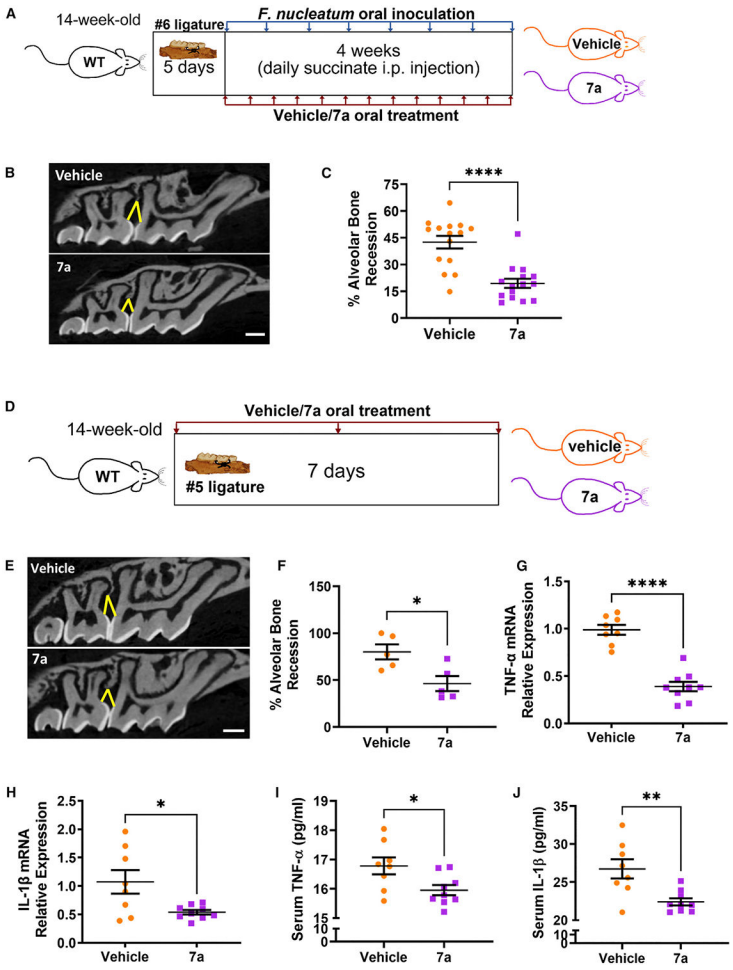

Figure 5. Inhibitory effects of 7a gel formulation *in vivo*

(A) Experimental design for (B) and (C).

(B and C) Representative μCT images (B; scale bar, 500 μm); the distance between the cementoenamel junction (CEJ) and alveolar bone crest was measured using the maxilla μCT images in each animal (individual distance). The mean distance between the CEJ and alveolar bone crest determined in age-matched healthy WT mice (mean distance) was used to calculate the percentage of alveolar bone recession in each animal using the following formula: (individual distance – mean distance)/mean distance × 100%. Error bars show mean ± SEM. n = 15; ****p < 0.0001.

(D) Experimental design for (E)–(J).

(E and F) Representative μCT images (E; scale bar, 500 μm) and percentage of alveolar bone recession (F) in each group, calculated as described previously. Error bars show mean ± SEM. n = 5; *p < 0.05.

(G and H) TNF-α (G) and IL-1β (H) mRNA levels in the gingival tissues.

(I and J) TNF-α (I) and IL-1β (J) protein levels in the serum of each group. Error bars show mean ± SEM. n = 8–9; *p < 0.05, **p < 0.01, ****p < 0.0001.

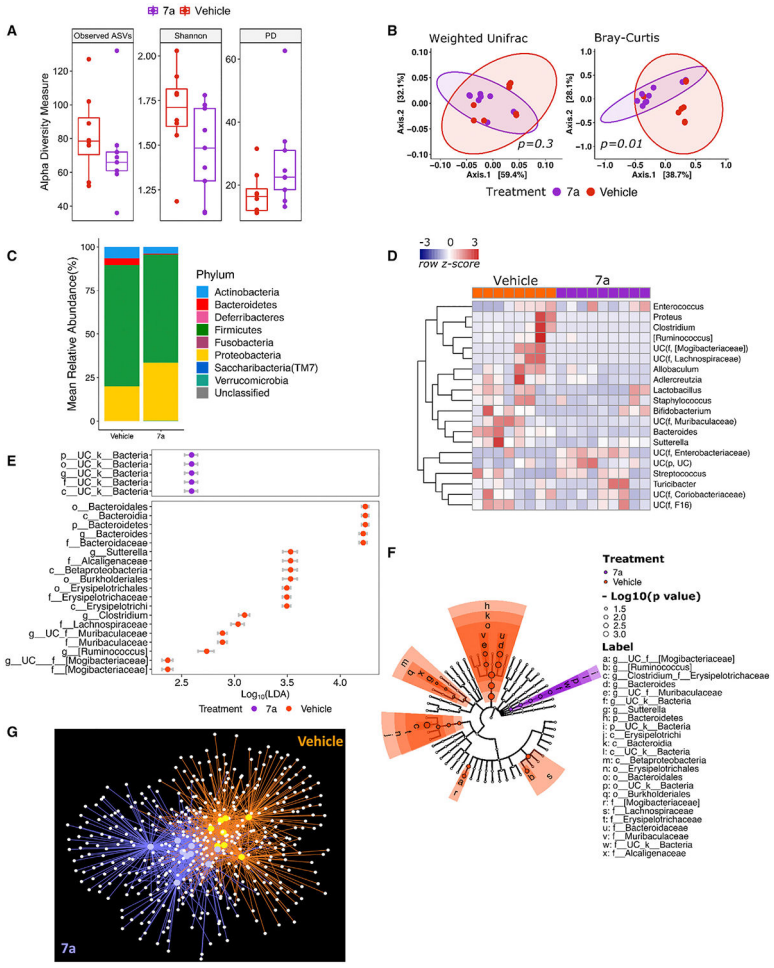

Figure 6. Application of 7a modulates the oral microbiota

(A) Alpha diversity measured by the observed number of ASVs, Shannon index, and phylogenetic diversity index for ligature samples from mice in the vehicle group (n = 8) and 7a-treated group (n = 9).

(B) PCoA for beta diversity based on the weighted UniFrac distance matrix and Bray-Curtis dissimilarity matrix (p = 0.01).

(C) Phylum-level relative abundance stacked bar plot showing bacterial community composition.

(D) Heatmap for the top 20 genera based on relative abundance normalized by row *Z* score. The higher taxon was added to the genus name when it was unclassified.

(E) Dot plot of the log-transformed linear discriminant analysis (LDA) score, showing the list of taxa that are statistically enriched in the study groups.

(F) Cladogram of the LDA results, showing phylogenetic relationships of the discriminative taxa in each group. Color represents taxa that were significantly more abundant in the corresponding group (7a in purple and vehicle in orange-red), and the size of the node indicates the negative base –10 logarithms of the p values.

(G) Network plot generated in Cytoscape 3.8.2 indicates a clear partition between the vehicle and 7a samples. The small white dots represent ASVs, the yellow dots represent

vehicle samples, the purple dots represent 7a samples, and edges represent the interaction between sample and ASV and are colored based on sample type.

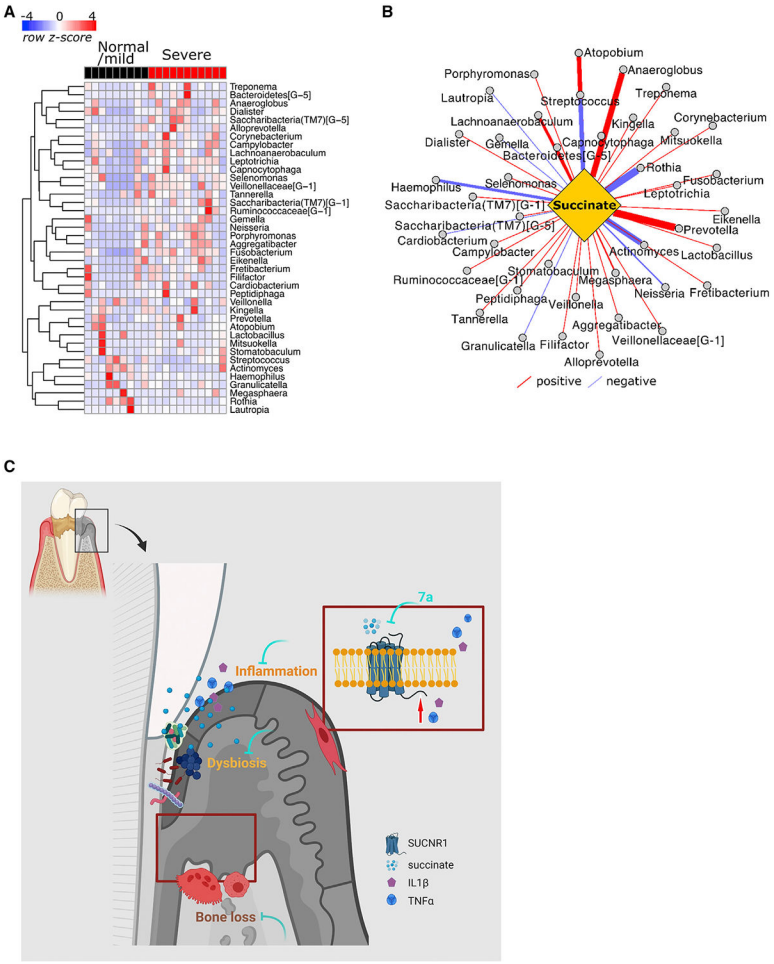

Figure 7. Succinate elevation correlates with periodontitis pathogens in affected individuals

(A) Heatmap for the top 40 genera based on relative abundance normalized by row Z score.

(B) Correlation-based network plot of the top 40 genera and succinate level in samples.

(C) Schematic summary of the role of succinate in manifestation of periodontitis; targeting SUCNR1 with 7a reduces the dysbiotic microbiome, periodontal inflammation, and bone loss; created with BioRender.

KEY RESOURCES TABLE

REAGENT or RESOURCE	SOURCE	IDENTIFIER
Antibodies		
GPR91 Antibody (SUCNR1)	Novus	Cat#:NBP1-00861; RRID:AB_1503315
Anti-GPR91 antibody	Abcam	Cat#:ab140795
Anti-rabbit IgG (H + L), F(ab')$_2$ Fragment (Alexa Fluor® 488 Conjugate)	Cell Signaling Technology	Cat# 4412; RRID:AB_1904025
Anti-rabbit IgG (H + L), F(ab')$_2$ Fragment (Alexa Fluor 594 Conjugate)	Cell Signaling Technology	Cat# 8889; RRID: AB_2716249
Bacterial and virus strains		
Fusobacterium nucleatum	ATCC	10953
E.coli	ATCC	25922GFP
Biological samples		
Human dental plaque	Dr. Saxena	N/A
Human gingival tissue	Dr. Saxena	(Pushalkar et al., 2014)
Murine serum	This study	N/A
Murine gingival ligature	This study	N/A
Murine oral swab	This study	N/A
Murine maxillae	This study	N/A
Murine gingival tissue from maxillae	This study	N/A
Murine bone marrow	This study	N/A
Chemicals, peptides, and recombinant proteins		
PBS	Gibco	14190-144 /14190-136
Succinate	Sigma	14160-100G
EDTA	Fisher Chemical	E478-1
BlockAid™ Blocking Solution	Invitrogen	B10710
DAPI	Cell Signaling Technology	4083
ActinGreen™ 488	Invitrogen	R37110
Sodium acetate	Sigma	S2889
L-(+) Tartaric acid	Sigma	T6521
Glacial acetic acid	Sigma	AX0077
Sodium hydroxide	Sigma	S5881
Napthol AS-MX Phosphate	Sigma	N4875
Fast Red Violet LB Salt	Sigma	F3381
Fast Green FCF	Fisher BioReagents	BP123-10
α-minimum Eagle's medium	HyClone	SH30265.01 /SH30265.02
Dulbecco's Modified Eagle's Medium	Sigma	D6429
FBS	Gibco	16000069
M-CSF	PeproTech	315-02
RANKL	PeproTech	315-11
TRIzol Reagent	Invitrogen	15596018
SYBR® Green	Applied Biosystems	4368708

REAGENT or RESOURCE	SOURCE	IDENTIFIER
DEPC	Sigma	D5758-25ML
Formalin	Sigma	HT501128-4L
PFA	Sigma	P6148-1KG
WGA	Invitrogen	W849
RNAscope® 2.5 LS Probe- Mm-Sucnr1-C3	ACD	437728-C3
Prolong Gold Antifade mountant	Invitrogen	P36934
Compound 7a	This study	N/A
LPS-P.g	InvivoGen	tlrl-pglps
Gel formulation vehicle	This study	N/A
Gel formulation 7a	This study	N/A
TE buffer	MasterPure	MTE0970
BD Trypticase™ soy agar plates with 5% sheep blood	BD biosciences	BD 221261
BBL brain heart infusion broth (modified)	BD biosciences	BD 299070
Critical commercial assays		
RNeasy Plus Mini Kit	Qiagen	74136
QIAamp PowerFecal DNA Kit	Qiagen	12830-50
TaqMan® reverse transcription Reagents	Invitrogen	N8080234
Succinate Assay Kit (Colorimetric)	Abcam	Ab204718
Acid Phosphatase, Leukocyte (TRAP) Kit	Sigma	387A-1KT
Mouse TNF-alpha Quantikine ELISA Kit	R&D Systems	MTA00B
Mouse IL-1 beta/IL-1 F2 Quantikine ELISA Kit	R&D Systems	MLB00C
RNAscope® LS Multiplex Fluorescent Reagent Kit	ACD	322800
V-PLEX Plus Proinflammatory Panel 1 Human Kit	MSD	K15049G
V-PLEX Proinflammatory Panel 1 Mouse Kit	MSD	K15048D
Quant-iT PicoGreen dsDNA Assay Kit	Invitrogen	P7589
KAPA HiFi HotStart ReadyMix	Roche	7958935001
Nextera XT Index Kit_ Set A	illumina	FC-131-2001
Nextera XT Index Kit_ Set B	illumina	FC-131-2002
MiSeq Reagent Kit v3 (600-cycle)	illumina	MS-102-3003
Deposited data		
Raw sequence data	This study	PRJNA772167
R code	This study	https://doi.org/10.5281/zenodo.7019470
Experimental models: Cell lines		
Human Gingival Fibroblast cells: HGF-1	ATCC	CRL-2014
Ready-to-Assay™ SUCNR1/GPR91 Succinate Receptor Frozen Cells Kit	Millipore	HTS241RTA
Experimental models: Organisms/strains		
C57BL/6J mice	Jackson Laboratory	000664
B6.FVB-Tg(EIIa-cre)C5379Lmgd/J	Jackson Laboratory	003724
SUCNR1 flox mice	This study (Cyagen & Taconic)	N/A
Software and algorithms		
GraphPad Prism (9.1.1)	GraphPad Software	www.graphpad.com

REAGENT or RESOURCE	SOURCE	IDENTIFIER
BioRender	BioRender	https://biorender.com/
ImageJ (1.8.0)	NIH Image	https://imagej.net/Fiji
Phenochart (1.0.11)	Akoya Biosciences	https://www.akoyabio.com/
Inform (2.4.11)	Akoya Biosciences	https://www.akoyabio.com/
OmeroInsight (1-1-0)	Open Microscopy Environment (OME)	https://www.openmicroscopy.org/
Omero Figure	Open Microscopy Environment (OME)	https://omero.nyumc.org/omero_plus/login/?url=%2Fwebclient%2F
NRecon (1.6.10.2)	Bruker microCT	https://www.brukersupport.com/
DataViewer (1.5.1.2)	Bruker microCT	https://www.brukersupport.com/
CTVox (2.7.0.0)	Bruker microCT	https://www.brukersupport.com/
DISCOVERY WORKBENCH (4.0)	MSD	https://www.mesoscale.com
QIIME 2 (v2020.2)	(Bolyen et al., 2019)	https://docs.qiime2.org/2020.2/
R (v4.0.5)	R for statistical computing and graphics	https://www.r-project.org/
Cytoscape(v3.8.2)	(Shannon et al., 2003)	https://github.com/cytoscape/cytoscape-tutorials/wiki
Metscape(v3.1.3)	(Basu et al., 2017)	http://metscape.ncibi.org/
Oligonucleotides		
See Table S1 for primers used in this study	N/A	N/A
Other		
Experimental Pathology Research Laboratory	NYU School of Medicine Langone Health	RRID:SCR_017928
Metabolomics Laboratory Core Facility	NYU School of Medicine Langone Health	RRID:SCR_017935
Micro CT Core	NYU CSCB	N/A